EuCARD

European Coordination for Accelerator Research and Development

PUBLICATION

HOM electronics and code to probe beam centring on 3.9 GHz cavities

Zhang, P (DESY)

19 June 2014

The electronic version of this EuCARD Publication is available via the EuCARD web site <http://cern.ch/eucard> or on the CERN Document Server at the following URL :
<http://cds.cern.ch/record/1710320>

EuCARD

HOM ELECTRONICS AND CODE TO
PROBE BEAM CENTRING
ON 3.9 GHZ CAVITIES

Doc. Identifier:
EuCARD-D10 **5 1-report-FINAL-RMJ**

Date: 17/07/2013

Grant Agreement No: 227579

EuCARD

European Coordination for Accelerator Research and Development

Seventh Framework Programme, Capacities Specific Programme, Research Infrastructures,
Combination of Collaborative Project and Coordination and Support Action

DELIVERABLE REPORT

HOM ELECTRONICS AND CODE TO PROBE BEAM CENTRING ON 3.9 GHZ CAVITIES

DELIVERABLE: D10.5.1

Document identifier:	EuCARD-D10 5 1-report-FINAL-RMJ
Due date of deliverable:	End of Month 48 (March 2013)
Report release date:	17/07/2013
Work package:	WP10: SRF – Superconducting Radio Frequency Technology
Lead beneficiary:	DESY
Document status:	Final

Abstract:

The work within sub-task 10.5.1 was aimed at developing electronics for beam position monitoring (BPM) based on Higher-Order Modes (HOM) excited by electron beams in 3.9 GHz cavities in the FLASH linac at DESY, Hamburg, defining realistic specifications and proving that these signals can be used for beam centering. A series of measurements with devices like a fast oscilloscopes and a real-time spectrum analyzer, as well as with specially designed test electronics. These measurements in conjunction with the simulations made by the other 2 sub-tasks have enabled us to find two spectra regions suitable for use as BPM: modes with strong coupling to the beam around 5.4 GHz, enabling precise monitoring

**HOM ELECTRONICS AND CODE TO
PROBE BEAM CENTRING
ON 3.9 GHZ CAVITIES**

Doc. Identifier:

EuCARD-D10 **5 1-report-FINAL-
RMJ**

Date: 17/07/2013

(resolution of ca 20 μm rms) within the whole 4-cavity module, and localized modes at ca. 9 GHz for localized measurements in each cavity (resolution of ca 50 mm rms). Various data analysis approaches have been studied. Based on the EuCARD work the HOMBPM electronics has been designed and is now being built at FNAL. The work of this task will be the starting point for the HOMBPM monitors for the 3.9 GHz cavities to be installed the European XFEL.

HOM ELECTRONICS AND CODE TO
PROBE BEAM CENTRING
ON 3.9 GHZ CAVITIES

Doc. Identifier:
EuCARD-D10 **5 1-report-FINAL-RMJ**

Date: 17/07/2013

Delivery Slip

	Name	**Partner**	**Date**
Authored by	P. Zhang	DESY	28/02/13
Reviewed by	R.M. Jones, N. Baboi	UMAN, DESY	16/07/13
Approved by WP Coordinator	O. Napoly	CEA	30/05/13
Approved by Project coordinator	Jean-Pierre Koutchouk		17/07/13

TABLE OF CONTENTS

1. EXECUTIVE SUMMARY

At the FLASH facility in DESY, 1.3 GHz (known as TESLA) and 3.9 GHz (third harmonic) cavities are installed. Beam-excited wakefields in the 3.9 GHz cavities are significantly larger than those in the 1.3 GHz cavities. It is therefore important to mitigate the adverse effects of higher-order modes (HOM) to the beam by aligning the beam on the electric axis of the 3.9 GHz cavities. Although previous HOMBPM electronics have been built for 1.3 GHz cavities, the four 3.9 GHz cavities within the module ACC39 posed several specific challenges: the frequencies are higher and many of the dipole modes within the cavities are coupled to all four cavities. This prevents isolating single modes and inter-cavity modes have to be consider, apart from a limited number of modes which are trapped within a single band.

A brief introduction to the FLASH accelerator and to the principle of beam position measurement using HOM signals is provided. This report is focussed on an analysis of the feasibility of an accurate measurement of beam position based on HOM signals either from simulation or from actual 3.9 MHz cavities, using laboratory instruments. Dependencies of HOMs in third harmonic cavities on transverse beam positions have been observed for the first time. Beam-pipe modes and trapped cavity modes in the fifth dipole band, and propagating cavity modes in the first two dipoles bands have been identified as appropriate frequency bands to measure the beam position in single cavities and four-cavity module. The measured resolution is in the order of hundreds of μm for both propagating and trapped modes. It is mainly limited by the resolution of the real-time spectrum analyzer used for the measurement. In order to overcome this limitation, dedicated test electronics for HOM-based beam diagnostics has been built for precise studies and assessment of the modal options. We measured resolutions of the order of 50 μm for single cavity and 20 μm for a four-cavity module were measured and this was achieved by building test electronics with band-pass filters focused on the modal frequencies of interest. Furthermore, based on this experience, a set of dedicated electronics is being built using modes in the second dipole band and the fifth dipole band, and we anticipate providing similar HOM diagnostics for the European XFEL third harmonic module consisting of eight cavities. In a final step, the algorithmic methods to extract the transverse beam position from the HOMs signal excited by the electron beam has been optimized in terms of resolution, computational efficiency and ability to measure the first bunch in a bunch train (short enough time window). These beam position resolutions have been obtained again using Single Value Decomposition (SVD) technique rather than traditional Least-Square method, and this allows for a large gain in computation time in the calibration phase. Measurements times corresponding to less than those of the inter-bunch spacing have been achieved.

2. INTRODUCTION

Higher order modes (HOM) are electromagnetic resonant fields. They can be excited by an electron beam entering an accelerating cavity, and constitute a component of the wakefield. This wakefield has the potential to dilute the beam quality and, in the worst case, result in a beam-break-up instability. It is therefore important to ensure that these fields are well suppressed by extracting energy through special couplers. In addition, the effect of the transverse wakefield can be reduced by aligning the beam on the cavity axis. This is due to their strength depending on the transverse offset of the excitation beam. For suitably small

HOM ELECTRONICS AND CODE TO PROBE BEAM CENTRING ON 3.9 GHZ CAVITIES

offsets the dominant components of the transverse wakefield are dipole modes, with a linear dependence on the transverse offset of the excitation bunch. This fact enables the transverse beam position inside the cavity to be determined by measuring the dipole modes extracted from the couplers, similar to a cavity beam position monitor (BPM), but requires no additional vacuum instrumentation.

At the FLASH facility in DESY, 1.3 GHz (known as TESLA) and 3.9 GHz (third harmonic) cavities are installed. Wakefields in 3.9 GHz cavities are significantly larger than in the 1.3 GHz cavities. It is therefore important to mitigate the adverse effects of HOMs to the beam by aligning the beam on the electric axis of the cavities. This alignment requires an accurate beam position diagnostics inside the 3.9 GHz cavities. It is this aspect that is focused on in this thesis. Although the principle of beam diagnostics with HOM has been demonstrated on 1.3 GHz cavities, the realization in 3.9 GHz cavities is considerably more challenging. This is due to the dense HOM spectrum and the relatively strong coupling of most HOMs amongst the four cavities in the third harmonic cryo-module.

A comprehensive series of simulations and HOM spectra measurements have been performed in order to study the modal band structure of the 3.9 GHz cavities. The dependencies of various dipole modes on the offset of the excitation beam were subsequently studied using a spectrum analyzer. Various data analysis methods were used: modal identification, direct linear regression, singular value decomposition and k-means clustering. These studies lead to three modal options promising for beam position diagnostics, upon which a set of test electronics has been built.

This chapter gives an overview of the FLASH facility and the ACC39 cryo-module, containing four 3.9 GHz cavities. The principle of using HOMs for beam position diagnostics is then introduced.

2.1. FLASH AND THE THIRD HARMONIC CAVITIES

FLASH is a free-electron laser facility at DESY providing electron bunches with high peak current to generate coherent light with unprecedented brilliance. It is also a test facility for various accelerator studies.
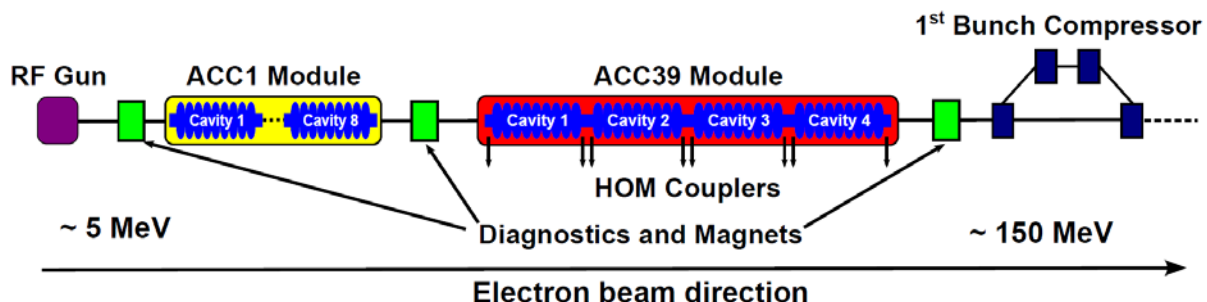
Fig. 1 Schematic of the injector section of FLASH facility.

Fig. 1 shows schematically the injector section of FLASH, which is relevant to our studies. The electron beam generated by a photoelectric gun is accelerated off-crest by eight superconducting 1.3 GHz TESLA cavities in cryo-module ACC1 and compressed by the first magnetic chicane. The electron bunch typically has a length of approximately 2 mm prior to entering the first bunch compressor. The bunches are supplied with a sinusoidal accelerating field and consequently a curvature develops in the energy-phase plane. This leads to a long

bunch tail and a reduction of peak current in the bunch compression. To linearize the RF field, harmonics of the fundamental accelerating frequency (1.3 GHz) of the main linac are added. At FLASH, third harmonic superconducting cavities operating at 3.9 GHz are used. Four such cavities are placed in the ACC39 module.

The ACC39 module is composed of four cavities namely C1 through C4 (illustrated in Fig. 2). Each cavity is equipped with two HOM couplers. By extracting HOMs through these couplers, the wakefields are well suppressed and their deleterious effects on the beam are minimized. Wakefields extracted from these couplers are guided by long cables to a HOM board rack outside the tunnel. After the module has been installed at FLASH, all the measurements were conducted from this rack.
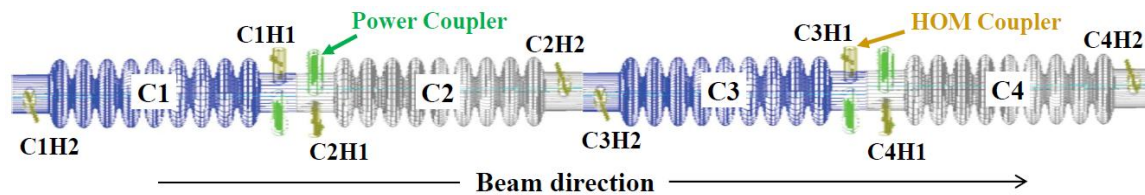

Fig. 2 Schematic of the four cavities within ACC39 module. The power couplers (green) are placed downstream for C1 and C3, and upstream for C2 and C4. The HOM couplers (brown) located on the same side of the power couplers are named H1, while the other ones H2.

The third harmonic 3.9 GHz cavity inherits a similar design of the 1.3 GHz TESLA cavity. A schematic of the third harmonic cavity is illustrated in Fig. 3(a) along with important dimensions. It has one power coupler and one pick-up probe installed on the beam pipe connecting end-cells. It is also equipped with two HOM couplers installed on each side of the connecting beam pipes with different rotations as shown in Fig. 3(b) and different designs. The HOM coupler located on the same side of the power coupler is named H1, while the other H2. The wakefields in the third harmonic 3.9 GHz cavity are significantly stronger than those in the TESLA 1.3 GHz cavity due to a much smaller iris radius: 15 mm compared with 35 mm. Unlike the TESLA 1.3 GHz cavity, most HOMs in the third harmonic 3.9 GHz cavity are above the cutoff frequencies of the connecting beam pipes in order to achieve a better damping of the HOM. However, this allows HOMs to propagate amongst cavities in the module, and thus gives rise to a dense coupled modal spectrum in the third harmonic cavity.
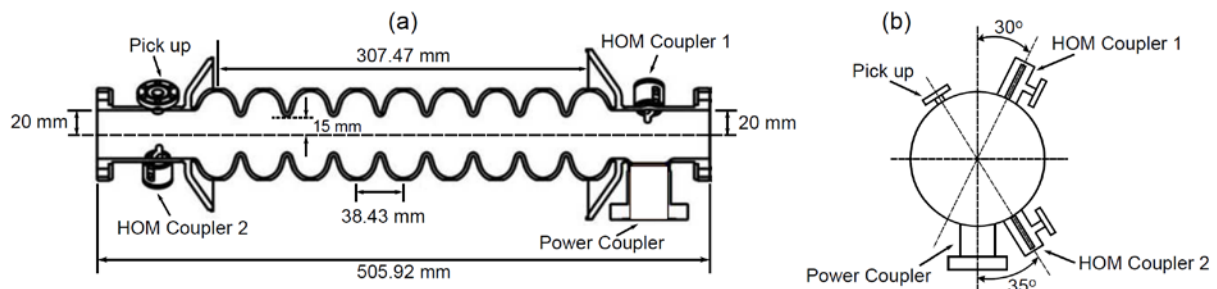

Fig. 3 Schematic of a third harmonic cavity with one power coupler, one pick up probe and two HOM couplers.

2.2. FUNDAMENTALS OF BEAM POSITION DIAGNOSTICS WITH HOM RADIATION

In order to describe the essential principle of the diagnostics, consider a simplified third harmonic cavity without couplers, which has cylindrical symmetry as shown in Fig. 4. In this

structure, a particle of point charge *q'* is moving in the *z* direction with an ultra-relativistic velocity *c*. The particle has a transverse offset *r'*, which is projected in Cartesian coordinates as *x'* and *y'*.
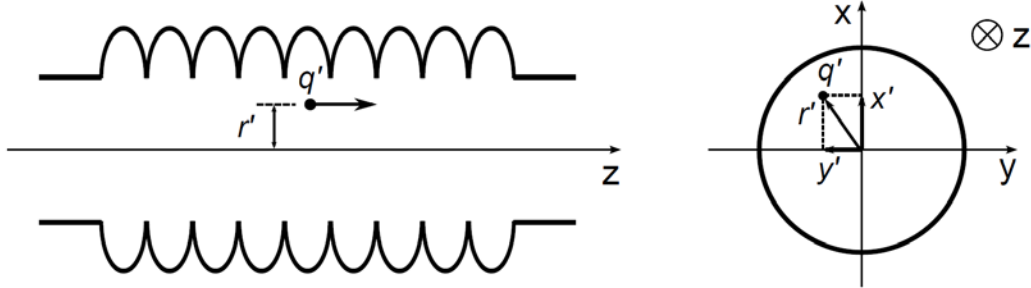

Fig. 4 A point charged particle q' traversing a cavity with an offset x' and y'.

As the particle q' traverses the cavity, a wakefield is excited. This beam-excited wakefield has both longitudinal and transverse components. The former has a direct impact on the energy spread of the beam and the latter results in an emittance dilution. For diagnostics purposes we concern ourselves with the transverse wakefield. In particular we focus on the long range wakefield - i.e. the electromagnetic fields that succeeding bunches in the train experience. Close to the axis where *r'* is small, the transverse wake potential $\vec{W}_\perp$ is dominated by dipole modes. Performing a multi-pole expansion, $\vec{W}_\perp$ can be written as

$$\vec{W}_\perp \approx (x'\vec{e}_x + y'\vec{e}_y)\, c \sum_n^\infty \left(\frac{R}{Q}\right)_n \sin\frac{\omega_n s}{c}, \quad \forall s > 0 \tag{1}$$

where $\vec{e}_x$ and $\vec{e}_y$ are unit vectors in *x* and *y* directions, $(R/Q)_n$ and ω_n are the ratio of shunt impedance to quality factor and radian frequency of the *n*th dipole eigenmode, *s* is the longitudinal position behind the particle *q'*. From this equation, $\vec{W}_\perp$ depends linearly on the transverse position *x'* and *y'* of the particle *q'* inducing the wakefield. This makes it possible to determine the transverse beam position inside the cavity by examining the beam-excited dipole signal.

3. FEASIBILITY STUDY

We investigate the feasibility of beam position diagnostics using higher order mode (HOM) signals excited by an electron beam in the third harmonic 3.9 GHz superconducting accelerating cavities at FLASH. After careful theoretical and experimental assessment of the HOM spectrum, three modal choices have been narrowed down to fulfill different diagnostics requirements. These are localized dipole beam-pipe modes, trapped cavity modes from the fifth dipole band, and propagating modes from the first two dipole bands. These modes are treated with various data analysis techniques: modal identification, direct linear regression (DLR), and singular value decomposition (SVD). Promising options for beam diagnostics are found from all three modal choices. This constitutes the first prediction, subsequently confirmed by experiments, of trapped HOMs in third harmonic cavities, and also the first direct comparison of DLR and SVD in the analysis of HOM-based beam diagnostics.

3.1. INTRODUCTION

Compared to the TESLA 1.3 GHz cavity, wakefields are significantly larger in the third harmonic 3.9 GHz cavity. Therefore, it is important to minimize these fields by aligning the beam with respect to the electrical axis of the cavity. This relies on accurate beam position diagnostics inside each cavity. However, conventional diagnostics instrumentations such as beam position monitors (BPMs) fall short of providing this information directly. Energy radiated to the HOM couplers of the cavity is capable of providing this information along with dedicated electronics. Prior to developing electronics, it is essential to characterize the HOMs and understand their behavior relating to beam offset. For this purpose, HOM measurements, both with and without beam excitations, were conducted. Simulations of the cavities, both with and without couplers, were also performed using various techniques. HOMs were extensively studied so as to search appropriate modes for diagnostics. Three modal choices have been narrowed down and their position dependencies on the beam are studied. Localized dipole beam-pipe modes and trapped cavity modes from the fifth dipole band are suitable for local position determination in each individual component (beam pipe or cavity). On the other hand, propagating modes from the first two dipole bands enable the beam position to be determined more precisely for an entire four cavity module, due to their strong coupling to the beam. Thus, coupled modes and trapped modes provide complementary information.

The next section proceeds with the HOM measurements of the third harmonic cavities both with and without beam excitation, together with eigenmode simulations. HOMs are identified and the inter-cavity coupling effects observed in measurements and simulations are described. Detailed studies of HOM dependence on the beam offset for various modes are described in Section 3.3. Final remarks constitute Section 3.4. Several data analysis techniques are used throughout the paper: a Lorentzian fit, linear regression, and singular value decomposition. A direct comparison of direct linear regression and singular value decomposition is presented for the first time in the study of HOM-based beam diagnostics. The potential for using these techniques to measure beam position is described. The relative merits of each dipole band in these techniques are carefully elucidated with reference to experiments conducted at FLASH.

3.2. MEASUREMENTS OF THE HOM SPECTRUM

In order to understand the HOM spectra of third harmonic cavities, modal characterization is needed at all stages after the fabrication of cavities: transmission spectra between two HOM couplers measured for each isolated single cavity are presented in Section 3.2.1, module-based transmission measurements in Section 3.2.2 and beam-excited HOM measurements in Section 3.2.3. The signals were measured from all eight HOM couplers. Not all measured signals are shown in this chapter. The selection is based on a representative sample of the typical behaviour of the modes. In particular, trapped modes and inter-cavity coupled modes are focused on with a view to understanding their application to HOM-based beam diagnostics.

3.2.1. Transmission spectra of an isolated single cavity

Third harmonic cavities were mounted on the test stand and cooled down at Fermilab after fabrication. The RF transmission spectrum (S_{21}) was subsequently measured for each isolated single cavity as shown schematically in Fig. 5. A typical spectrum is shown in Fig. 6(a) along with simulations of an ideal single cavity without couplers. The band structure of a single

cavity is depicted in terms of monopole, dipole, quadrupole and sextupole modes from 3.7 to 10 GHz frequency span. As it will be explained later, regions of particular interests are respectively the fundamental band (Fig. 6(b)), the first two dipole bands (Fig. 6(d)) and the fifth dipole band (Fig. 6(c)). The nine modes in the fundamental band can be identified in Fig. 6(b). The accelerating mode is the last peak at 3.9 GHz (π mode). Unlike the simulated cavity, the actual cavity has couplers, which breaks the symmetry of the structure. This accounts for the differences between simulations and measurements. A direct simulation of a real cavity with couplers is computationally very expensive in terms of time and resources, thus alternative techniques were applied. In addition, other sources such as fabrication errors and cavity tuning can also contribute to the differences. The dipole modes are not readily identifiable as shown in Fig. 6(c) and Fig. 6(d).
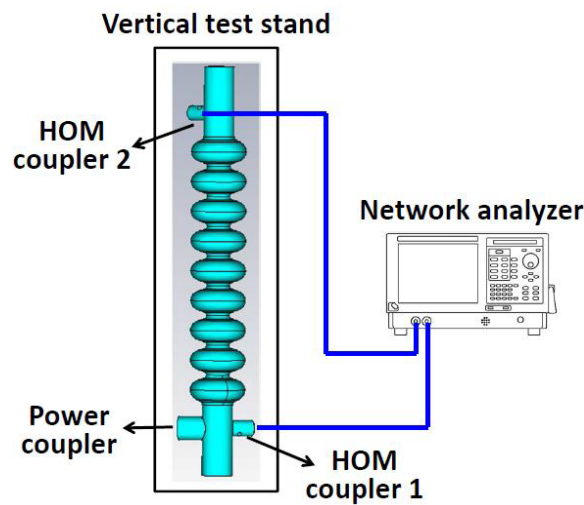

Fig. 5 The schematic setup of the single cavity RF measurement.

Fig. 6(a) Measured across C1 from C1H1 to C1H2

EuCARD

**HOM ELECTRONICS AND CODE TO
PROBE BEAM CENTRING
ON 3.9 GHZ CAVITIES**

Doc. Identifier:

EuCARD-D10 **5 1-report-FINAL-
RMJ**

Date: 17/07/2013
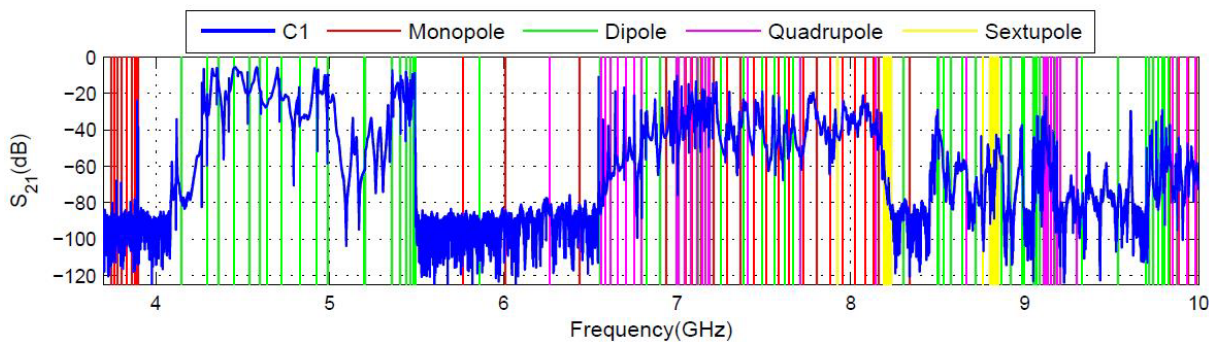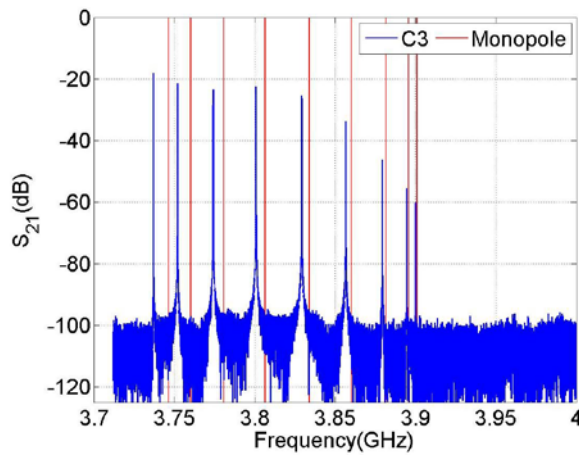
Fig. 6(b) The fundamental band
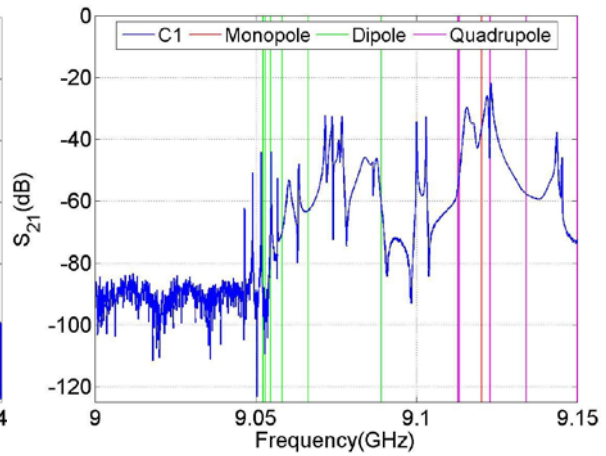
Fig. 6(c) The fifth dipole band
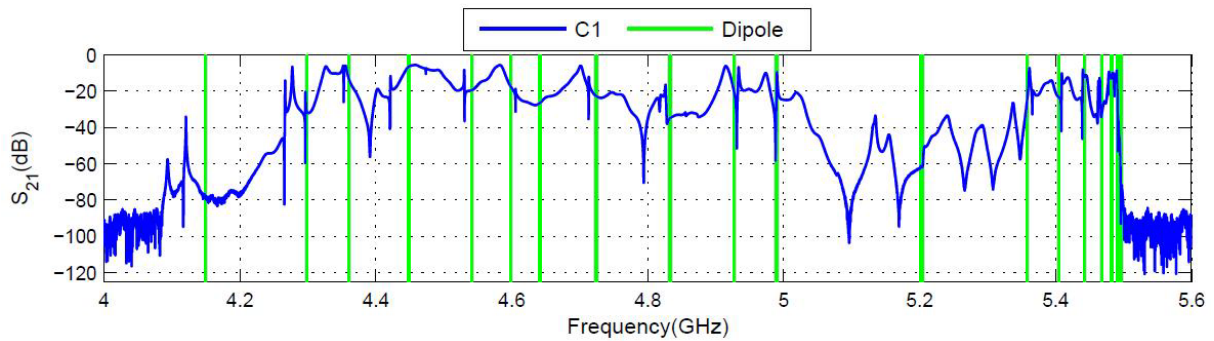
Fig. 6(d) The first two dipole bands

Fig. 6 Typical transmission spectrum (S21) of a single isolated cavity. The vertical lines indicate simulation results of eigenmodes.

For comparison, a typical beam-excited spectrum of the first dipole band of the TESLA 1.3 GHz cavity is shown in Fig. 7. Here one can identify nine peaks, which are clearly separated from each other. Mode #6 at approximately 1.7 GHz was used for HOMBPM in 1.3 GHz cavities. The *R/Q* of this mode is 5.54 Ω/cm^2. The modal spectrum is more complicated for the 3.9 GHz cavity (see Fig. 6(d)). Mode identification is by no means straightforward.

HOM ELECTRONICS AND CODE TO
PROBE BEAM CENTRING
ON 3.9 GHZ CAVITIES

Doc. Identifier:

EuCARD-D10 **5 1-report-FINAL-RMJ**

Date: 17/07/2013

Fig. 7 The beam-excited spectrum of the first dipole band of the TESLA 1.3 GHz cavity. The spectrum was measured from HOM coupler C6H2 of the ACC1 module (see Fig. 2).

In general, each peak in Fig. 6 can be fit to a Lorentzian distribution:

$$y = \frac{y_0}{1 + \left(\dfrac{f - f_0}{\Delta f}\right)^2} \tag{2}$$

Here y_0 is the mode amplitude, f_0 is the center frequency and Δf is the half-width at half-amplitude (HWHM). In order to identify peaks in a complex sp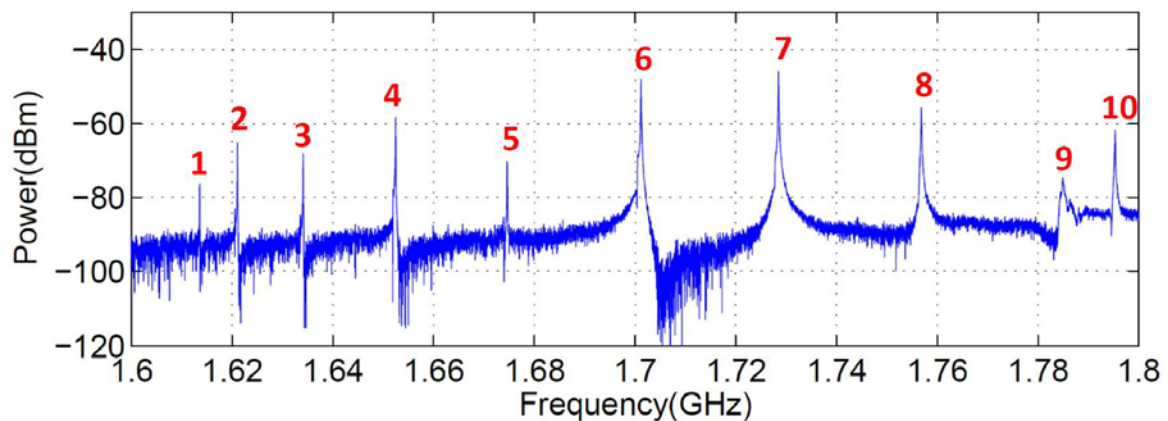ectrum, all modes in a dipole band are fit simultaneously rather than fitting individual peaks. The frequency f_0 and the quality factor Q ($Q = f_0/(2\Delta f)$) are then obtained for each mode. Fig. 8(a) shows the fitting results of the second dipole band using the commercial code PeakFit. On the top half of Fig. 8(a), the original spectrum is plotted in dotted line while the fitted one in solid line. On the bottom half, each peak denotes a mode with a fitted frequency marked on top. Hidden peaks are revealed. The goodness of fit is measured by the coefficient of determination r^2 ($r^2 = 1$, perfect fit; $r^2 = 0$, poor fit). The Q of each mode is shown in Fig. 8(b) along with the coupling strength to the beam for each mode from simulations. The Q_{ext} is also shown for each mode simulated on a cavity with power and HOM couplers. The total damping of a cavity mode is not only determined by finite resistance of the cavity wall (denoted by Q) but also by the external quality factor, Q_{ext}, which characterizes the coupling to HOM couplers. The polarization split of dipole modes and the frequency shift from ideal simulations can be observed. By comparing the modal frequencies between simulations and measurements, modes can be approximately identified, but this is by no means as straightforward or precise as it was with the TESLA-style cavities. In reality the cavities are connected through beam pipes within a module. The connecting beam pipes are above cut-off of the TE/TM dipole modes. It is important to characterize these coupling modes within a module. This is described in the next section.
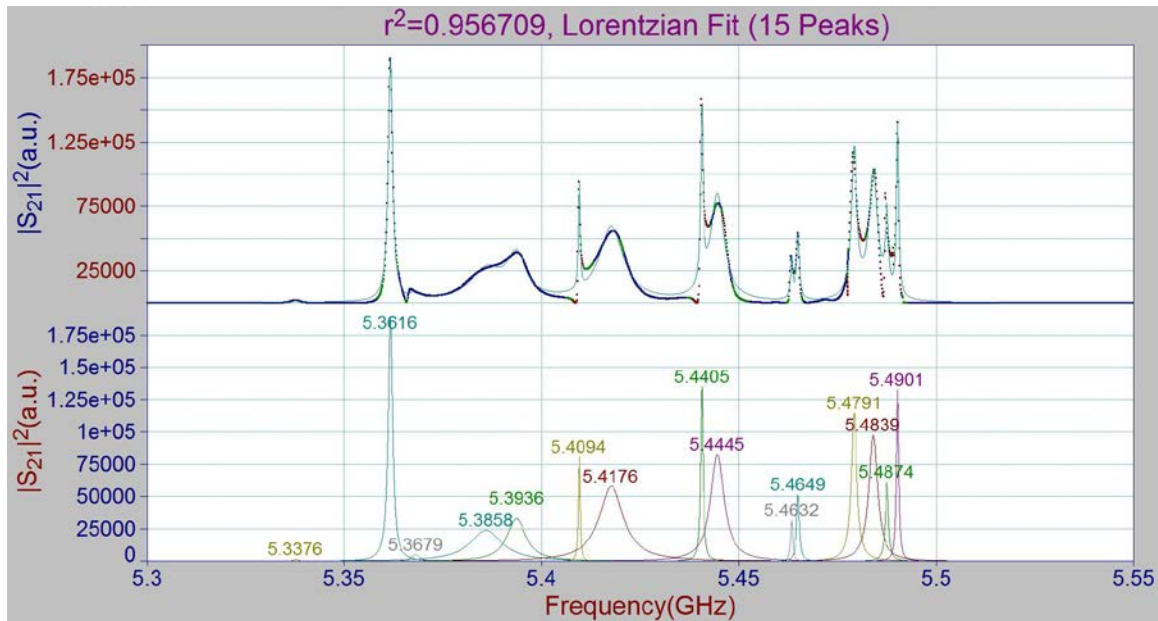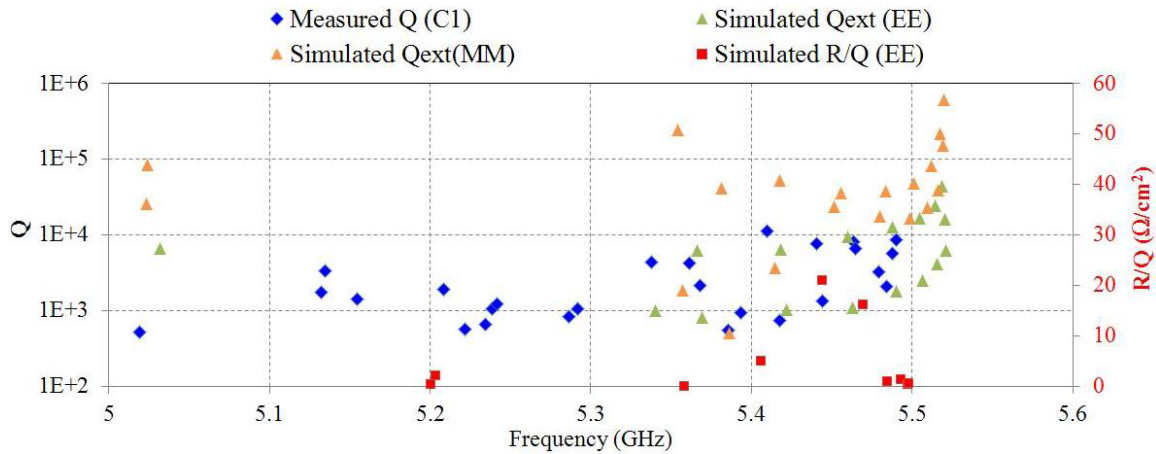

Fig. 8(a) Lorentzian fit

Fig. 8(b) Fit results compared with simulations

Fig. 8 Fit of the second dipole band of C1 (from the isolated single cavity measurement) as Lorentzian distributions and compared with simulations.

3.2.2. Module-based transmission spectra

After the assembly of all four cavities into the cryo-module ACC39, the module was installed in the Cryo-Module Test Bench (CMTB) at DESY. RF transmission measurements were conducted in the CMTB tunnel as shown schematically in Fig. 9. The measurements were repeated after the installation in FLASH from the HOM board rack outside the tunnel. HOM signals are stronger in CMTB than in FLASH because additional amplifiers were used and the cables are shorter. The two measurements are otherwise similar. Therefore CMTB results are shown regarding most of the module-based measurements without beam-excitation. From the recorded spectra, monopole, dipole and quadrupole bands are identified. Instead of usual discrete modes in the isolated single cavity spectrum described in Section 3.2.1, more modes arise due to the coupling of inter-connected cavities.
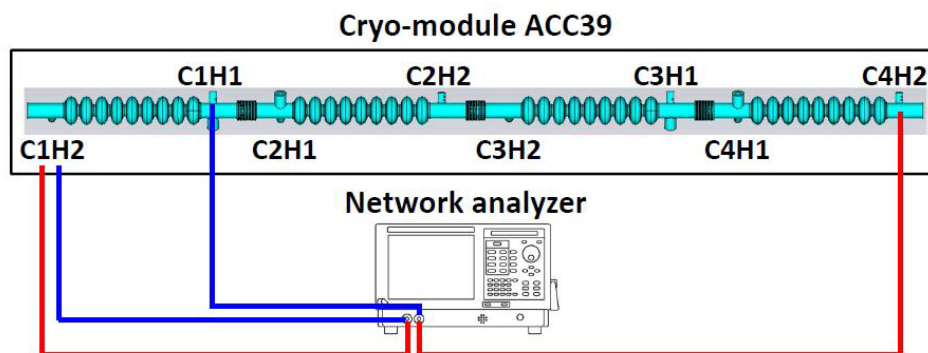
Fig. 9 The schematic setup of the module-based RF measurement.

In order to characterize the inter-cavity couplings of these modes, transmission spectrum was measured along the entire four-cavity string (from C1H2 to C4H2), and then compared with the spectra measured between upstream and downstream couplers of each cavity within the cryo-module. As expected from simulations, most HOMs couple to adjacent cavities through attached beam pipes. This can be observed in Fig. 10, where only a small portion of modes is below the cutoff frequencies of attached beam pipes (peaks present only in the cavity C1

**HOM ELECTRONICS AND CODE TO
PROBE BEAM CENTRING
ON 3.9 GHZ CAVITIES**

Doc. Identifier:

EuCARD-D10 **5 1-report-FINAL-
RMJ**

Date: 17/07/2013

spectrum but absent from the string spectrum). The theoretical cutoff frequency of the beam pipe is 4.39 GHz for dipole TE_{11} modes, while the measurement shows an even lower value at approximately 4.25 GHz. This might be due to the asymmetric geometry due to couplers and to fabrication tolerances. Dipole beam-pipe modes at approximately 4.1 GHz and cavity modes in the fifth dipole band at approximately 9.05 GHz are clearly visible as localized within each beam pipe or cavity.

Fig. 10(a) Spectrum from 3.7 to 9 GHz

Fig. 10(b) The fifth dipole band

Fig. 10 Couplings of inter-connected cavities. The measurements were made at CMTB, while the spectra measured across C1 (from C1H1 to C1H2) is in blue, and the spectra measured across the entire four-cavity string (from C1H2 to C4H2) is in red.
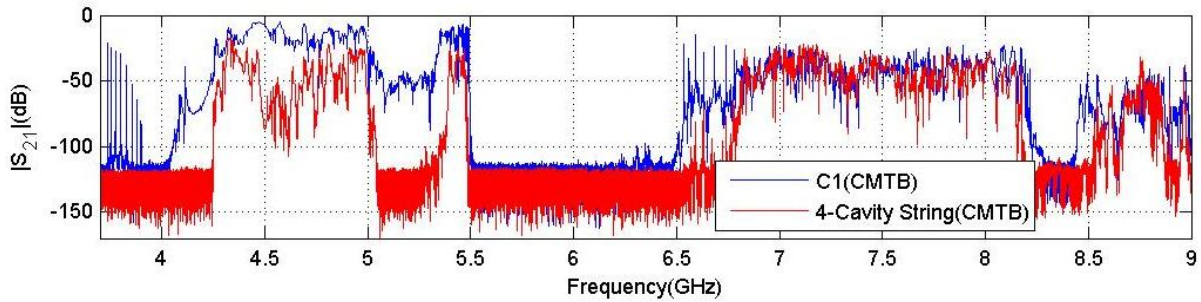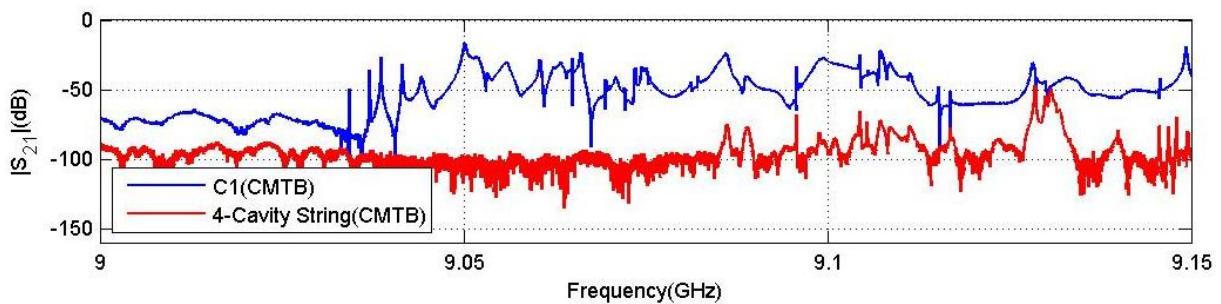
3.2.3. Beam-Excited HOM Spectra

The beam-excited spectra measurement at FLASH was conducted using a Tektronix Oscilloscope (scope) with a bandwidth of 6 GHz and a Tektronix Real-time Spectrum Analyzer (RSA). As shown in Fig. 11, HOM signals were taken from both HOM couplers of all four cavities at ACC39 HOM patch panel outside the tunnel. A 10 dB external attenuator was connected to each HOM coupler to reduce the power of the beam-excited signals radiated to the coupler and thus protecting the devices. A RF multiplexer was used to connect one coupler to either the scope or the RSA during each measurement. Both the scope and the RSA were triggered by a 10 Hz RF signal delivered by the FLASH timing system, synchronized with the beam pulse. We were running FLASH with one bunch per beam pulse in a repetition rate of 10 Hz. The bunch charge was approximately 0.5 nC. A MATLAB script was used to control the RF multiplexer, the scope and the RSA as well as the data recording to the local computer hard disk. Time-domain waveforms and real-time spectra were recorded. Each waveform was sampled with 20 GS/s, and 200,000 points were recorded in a time window of 10 µs. Example waveforms from the upstream and the downstream couplers of C2 are shown in Fig. 12.

**HOM ELECTRONICS AND CODE TO
PROBE BEAM CENTRING
ON 3.9 GHZ CAVITIES**

Doc. Identifier:
EuCARD-D10 **5 1-report-FINAL-
RMJ**

Date: 17/07/2013
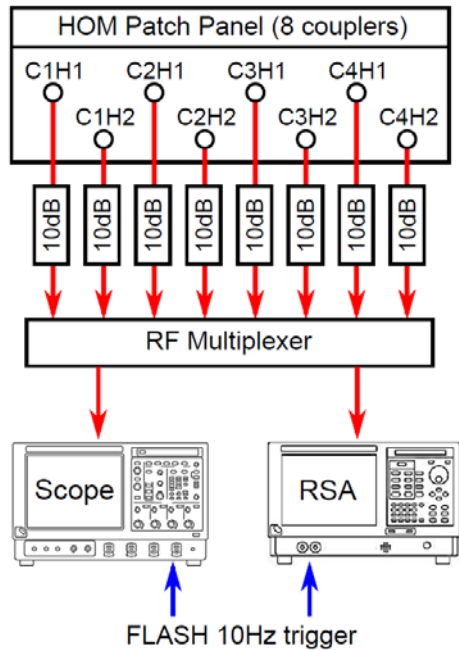
Fig. 11 Schematic setup for the beam-excited HOM measurements. The 10 dB external attenuators have been removed during the measurement of the fifth dipole band.
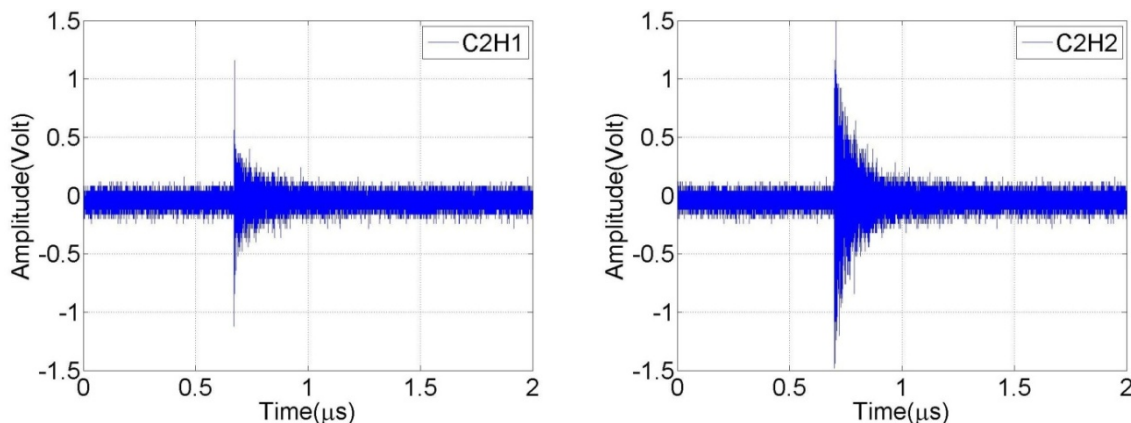
Fig. 12 Waveforms excited by a single electron bunch measured from the upstream and the downstream HOM coupler of C2.

The RSA has the capability to capture the HOM signal excited by a single bunch in a large bandwidth with a high frequency resolution. In our case, the acquisition bandwidth was set to 60 MHz with an acquisition length of 100 µs. A frequency step of 10 kHz and a resolution bandwidth of 22.5 kHz were used. The frequency span was set to 50 MHz. Starting from 4.025 GHz, the centre frequency was raised in a step of 50 MHz. Thus the spectral ranges were consecutively recorded. Each 50 MHz slice of the spectrum corresponds to a single bunch excitation. Fig. 13(a)(b) shows the beam-excited spectrum of the localized dipole beam-pipe modes and the first two dipole bands. The spectrum of the fifth dipole band is presented in Fig. 13(c) (without 10 dB external attenuator).

**HOM ELECTRONICS AND CODE TO
PROBE BEAM CENTRING
ON 3.9 GHZ CAVITIES**

Doc. Identifier:

EuCARD-D10 **5 1-report-FINAL-
RMJ**

Date: 17/07/2013
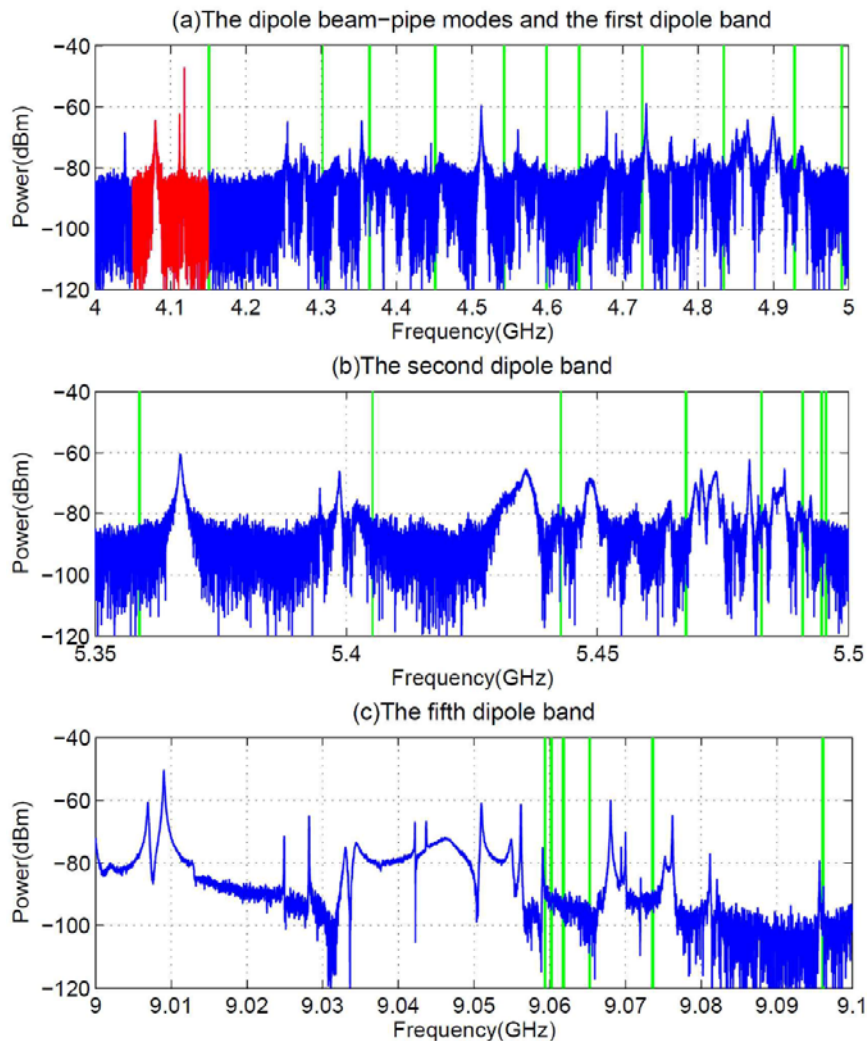
Fig. 13 Beam-excited spectra measured from HOM coupler C2H2 using RSA. The localized dipole beam-pipe modes are marked in red. The vertical lines denote dipole eigenmodes from simulations.

After this series of HOM spectra measurements, the band structure of modes has been characterized. Two categories of dipole modes of the third harmonic cavities have been distinguished. Modes in one category are localized in each cavity or segment of beam pipe, while in another category are propagating through the entire four-cavity module. Localized dipole modes consist of beam-pipe modes at approximately 4 GHz and some cavities modes in the fifth dipole band at approximately 9 GHz. These modes only possess small R/Q values according to simulations. Coupled dipole modes with large R/Q values consist of cavity modes in the first two dipole bands within 4.5 - 5.5 GHz. These two categories of modes are of particular interests for beam position diagnostics. Their dependencies on transverse beam offsets will be studied in the next section. Data analysis techniques used to extract beam position information from HOM signals must be employed and these techniques will also be explained.

3.3. HOM DEPENDENCE ON THE BEAM OFFSET

After modal characterizations of the third harmonic cavities, experiments were conducted to find the correlation of dipole modes to the transverse beam position. Localized modes and coupled modes were studied. Various data analysis techniques were used: Lorentzian fit, linear regression, and singular value decomposition. Linear dependencies are found and shown in this section. The direct linear regression method and the singular value decomposition method are compared in terms of prediction accuracy for both trapped and coupled modes.

3.3.1. Measurement setup

The schematic of the measurement setup is shown in Fig. 14. An electron bunch of approximately 0.5 nC is accelerated on-crest through ACC1 before entering the ACC39 module. Two steering magnets located upstream of ACC1 are used to produce horizontal and vertical offsets of the electron bunch in ACC39. Two beam position monitors (BPM-A and BPM-B) are used to record transverse beam positions before and after ACC39. Switching off the accelerating field in ACC39 and all quadrupoles close to ACC39, a straight line trajectory of the electron bunch is produced between those two BPMs. Therefore, the transverse offset of the electron bunch in each cavity can be determined by interpolating the readouts of the two BPMs.
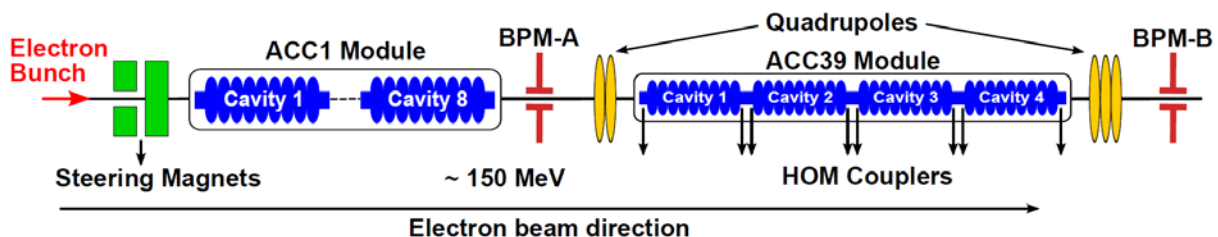
Fig. 14 Schematic of measurement setup for HOM dependence study (not to scale, cavities in ACC1 are approximately three times larger than those in ACC39).

For each beam position, along with HOM signals, nearby toroids, BPMs, and currents of steering magnets are also recorded synchronously. The electron bunch is moved in two dimensional (2D) cross manner and 2D grid manner. The steerers induce changes in beam offset and trajectory angle in ACC39. Due to technical difficulties to create trajectory angle in ACC39 independently and the contribution of the angle wakefield being much smaller than that of the offset wakefield, the angle is not considered in this study. The readings from BPM-A for these two scans are shown in Fig. 15. Position interpolations are applicable throughout Section 3.3 except the 2D cross scan (Fig. 15(a)) used for measuring beampipe modes. In this case, the quadrupoles between BPM-A and BPM-B were still on. One notices some tilt of the position readings during both scans. This is due to the coupling between *x* and *y* plane caused partially by the ACC1 module and partially by BPM-A itself.
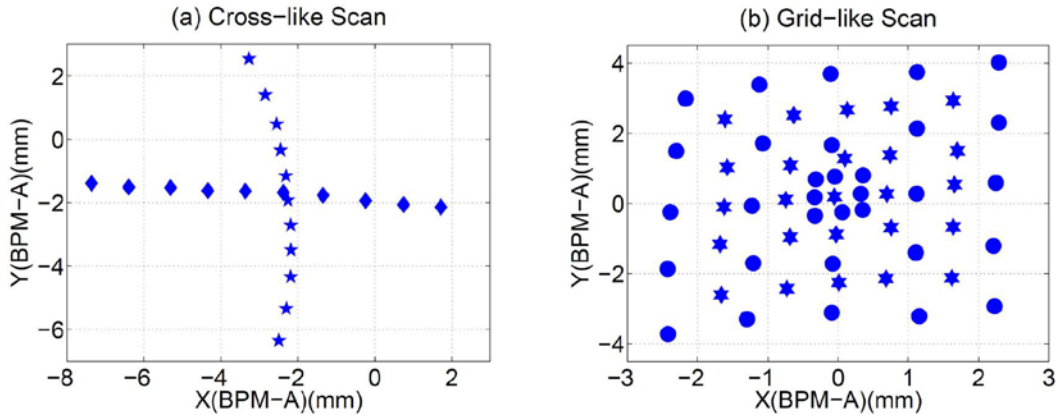
Fig. 15 Readings of BPM-A during beam scan.

3.3.2. Localized dipole beam-pipe modes

The spectra of two modes at approximately 4.1 GHz measured from C2H2 at ten different horizontal beam positions (diamonds in Fig. 15(a)) are shown in Fig. 16. They are identified as dipole beam-pipe modes. The vertical position reading from BPM-A was varied by ±0.24 mm during the horizontal scan. Variations of the mode amplitude with respect to the horizontal beam position can be observed. The amplitudes have been normalized to the beam charge. The amplitudes do not reach zero, which might be due to an offset in the vertical direction during the horizontal scan. In addition, other sources such as fabrication errors and cell misalignment can also contribute.
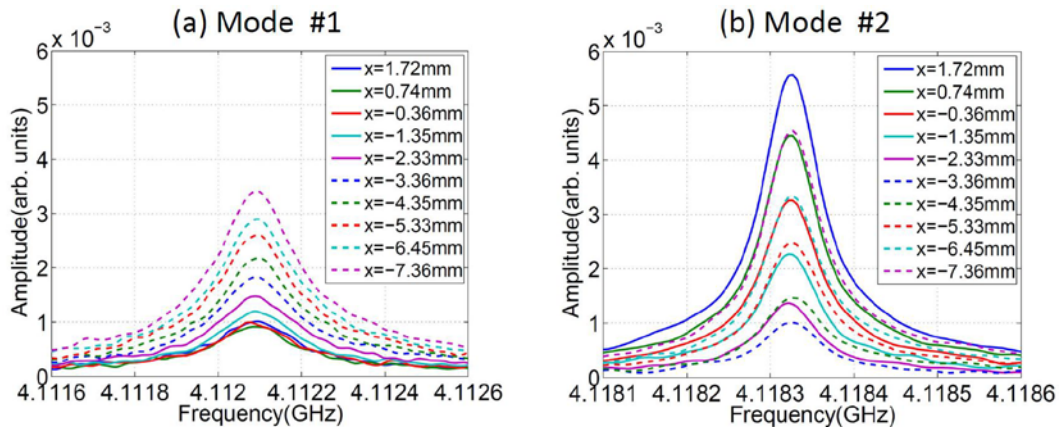
Fig. 16 Amplitude of dipole beam-pipe modes varies with transverse beam position read from BPM-A. The spectra were measured from HOM coupler C2H2.

Each mode corresponds to a resonant peak in the spectrum and is fit to the Lorentzian distribution (Eq. 2). Fig. 17 shows the amplitude of each mode as a function of the transverse beam position read from BPM-A for both horizontal and vertical beam scans (Fig. 15(a)). A linear dependence of the mode amplitude on the transverse beam position can be observed, which indicates dipole-like behaviour.

**HOM ELECTRONICS AND CODE TO
PROBE BEAM CENTRING
ON 3.9 GHZ CAVITIES**

Doc. Identifier:

EuCARD-D10 **5 1-report-FINAL-
RMJ**

Date: 17/07/2013

Fig. 17 Amplitude of dipole beam-pipe modes as a function of the transverse beam position read from BPM-A.

The polarization of each dipole beam-pipe mode is shown in Fig. 18, where the amplitude was measured in the 2D grid scan (Fig. 15(b)). Position interpolations from the two BPM readouts (BPM-A and BPM-B) are applied to get the transverse beam positions in the related beam pipe. These two modes are polarized perpendicularly, which indicates potential splitting of the mode degeneracy. This is also representative of dipole-like behaviour. The symmetry of the ideal cylindrical structure is broken by the HOM couplers installed on the connecting beam pipes. This causes the frequency split of the two polarizations along with the inevitable manufacturing tolerances. There are three beam pipes inter-connecting cavities in ACC39 (see Fig. 2), but clear polarizations can only be observed from the beam pipe connecting C2 and C3. The power couplers installed on the other two beam pipes may account for this.
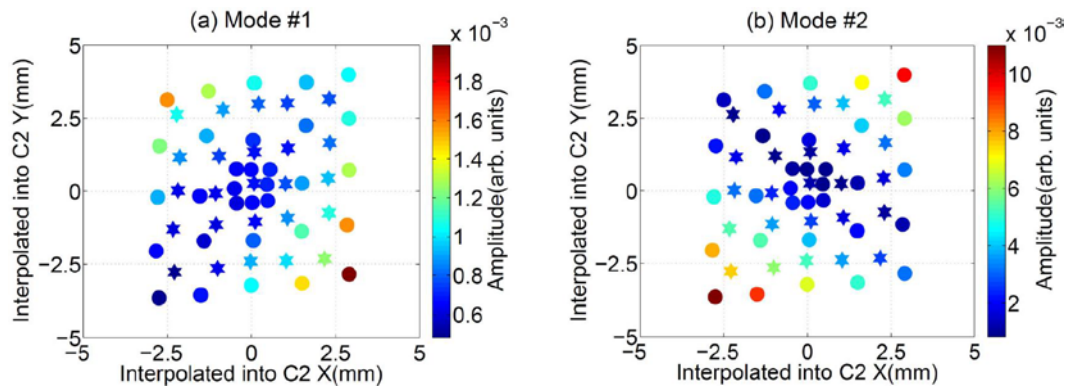
Fig. 18 Amplitude of dipole beam-pipe modes as a function of the transverse beam position interpolated into C2.

3.3.3. Trapped cavity modes in the fifth dipole band

As explained in Sec. II, trapped cavity modes exist in the fifth dipole band. By moving the beam horizontally, the variation of the amplitude of a mode at approximately 9.053 GHz can be clearly seen in Fig. 19(a). The vertical position in C1 varied by ±0.3 mm during this horizontal scan. Using a Lorentzian fit to obtain the amplitudes of the modes and plotting against horizontal beam positions interpolated from BPM readouts, the linear dependence can be clearly seen in Fig. 19(b), which indicates a dipole-like behaviour.

**HOM ELECTRONICS AND CODE TO
PROBE BEAM CENTRING
ON 3.9 GHZ CAVITIES**

Doc. Identifier:
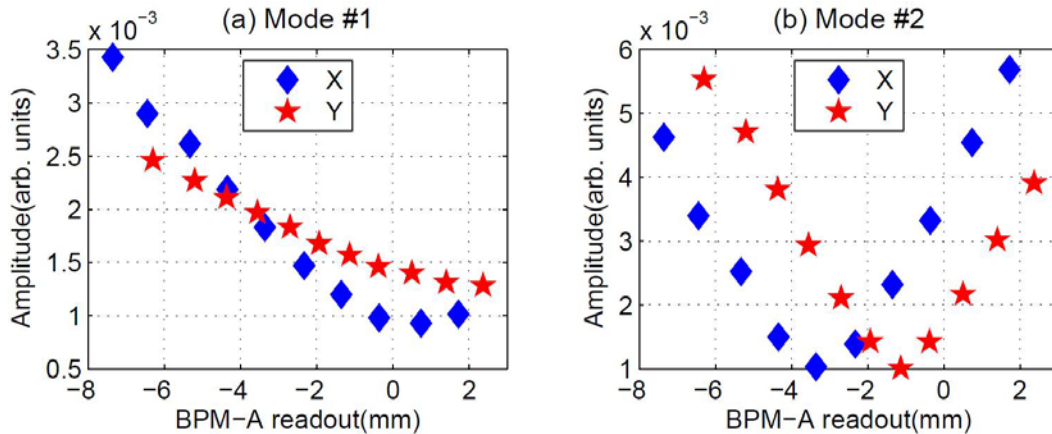
EuCARD-D10 **5 1-report-FINAL-
RMJ**

Date: 17/07/2013
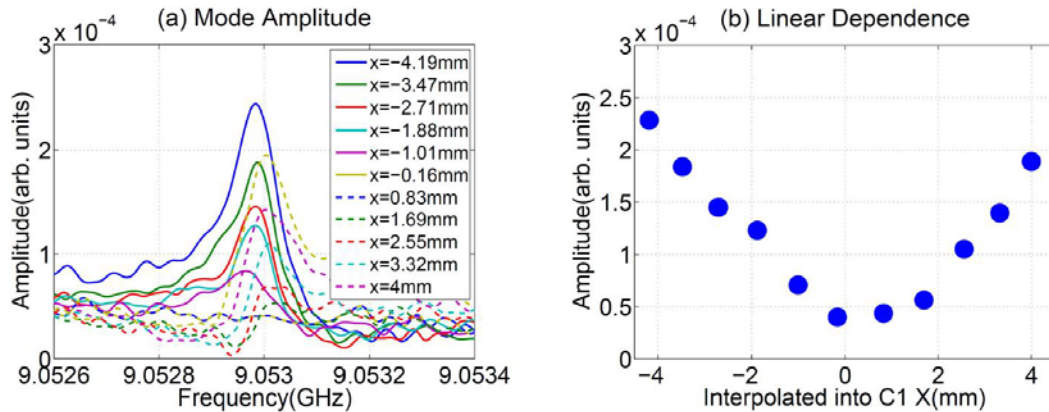
Fig. 19 Amplitudes of one dipole mode as a function of the transverse beam position interpolated into C1. The signals are measured from HOM coupler C1H1.

In general, modes in the fifth dipole band have small amplitude, therefore a dedicated grid-like beam scan was conducted without the 10 dB external attenuators, which were used for other frequency bands. The interpolated beam positions are shown in Fig. 20(a). The amplitude of the same mode at approximately 9.053 GHz is again obtained by a Lorentzian fit for each beam position, and plotted in Fig. 20(b). The colour denotes the amplitude magnitude. The polarization of this mode can be observed.
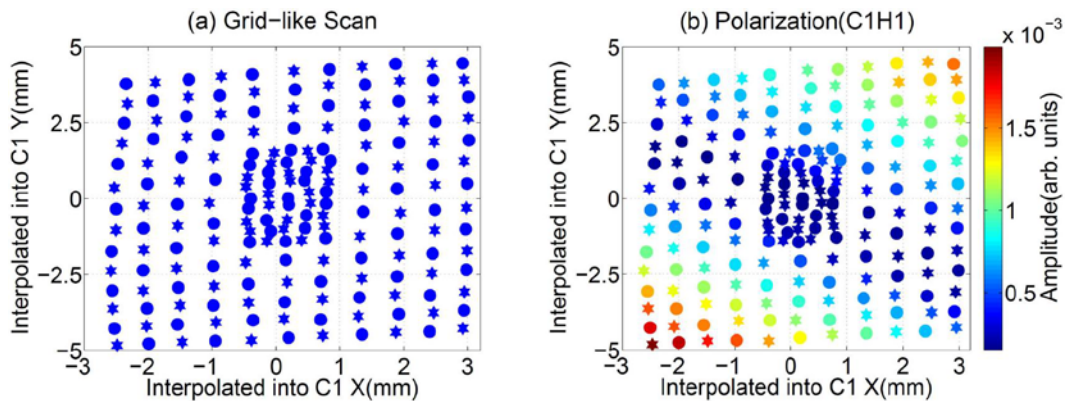
Fig. 20 (a) Grid-like beam scan. The positions are interpolated into C1. (b) Mode polarization (frequency: 9.053 GHz). The signals were measured from HOM coupler C1H1.

Spectra shown in Fig. 21 were recorded from all eight HOM couplers within the frequency range from 9.05 to 9.08 GHz. The spectrum from each HOM coupler of each cavity differs due to the fact that the HOM energy picked up by each coupler varies according to the detailed features of the individual couplers. As shown in Fig. 10(b), modes in this frequency range are trapped inside each cavity. Spectra within this bandwidth are therefore used for the following analysis.

**HOM ELECTRONICS AND CODE TO
PROBE BEAM CENTRING
ON 3.9 GHZ CAVITIES**

Doc. Identifier:

EuCARD-D10 **5 1-report-FINAL-RMJ**

Date: 17/07/2013
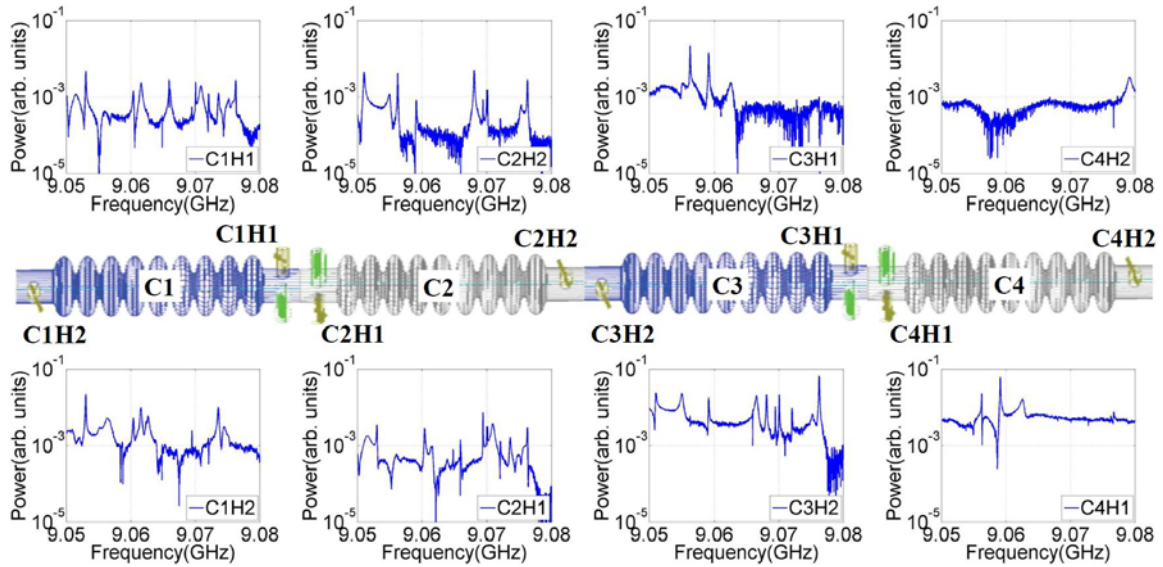
Fig. 21 Spectra measured from all eight HOM couplers of ACC39 module at one beam position.

- **Direct linear regression (DLR)**

Dipole modes have linear correlations to the transverse beam offset (Eq. 1). To extract beam position information from the dipole modes, a straightforward method is direct linear regression (DLR),

$$A \cdot M = B \tag{3}$$

In this equation, matrix A contains the magnitude of the HOM spectra (real and positive), B is the matrix of transverse beam position x and y interpolated from two BPM readouts. The angle of the beam trajectory x' and y' is not the subject of this study. M is the matrix of regression coefficients. Each row of A and B corresponds to one beam position. The intercept term for the regression is absorbed into A and M by adding one column of 1 in A and one row of coefficients in M. The matrix M is obtained by solving the linear system Eq. 3.

For the 2D grid beam scan, 184 samples (see Fig. 20(a)) are split equally into calibration samples (dots) and validation samples (hexagrams) in order to obtain full coverage in 2D space for both samples. The calibration samples are used to determine the matrix M, then the predictions of B can be obtained by applying matrix M on the validation sample. Applying DLR to the spectra measured from C1H1, we obtain the results for both samples. In Fig. 22(a), the prediction and the measurement almost overlap, which proves the linear dependence of spectra on transverse beam offset. The linearity is further validated in Fig. 22(b) when using the calibration on the validation samples. To measure the consistency, the coefficient of determination r^2 is calculated.

**HOM ELECTRONICS AND CODE TO
PROBE BEAM CENTRING
ON 3.9 GHZ CAVITIES**

Doc. Identifier:
EuCARD-D10 **5 1-report-FINAL-
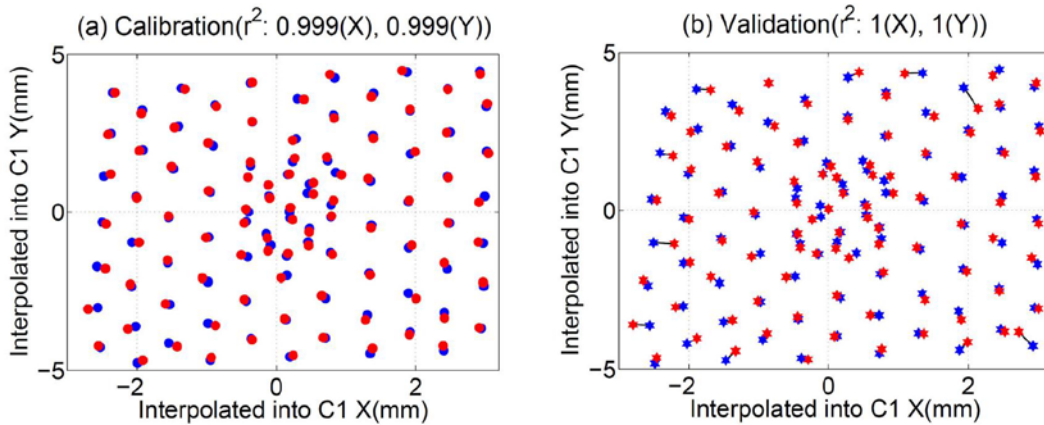RMJ**

Date: 17/07/2013

Fig. 22 Measurement (blue) and prediction (red) of the transverse beam position from calibration and validation samples (split as Fig. 20(a)). The method applied is DLR. Points connected with black lines belong to the same beam position.

The differences between the prediction and the measurement is defined as prediction error. Fig. 23 shows the prediction error for calibration and validation samples by using DLR. The root mean square (rms) of the prediction errors (rms errors) for the validation samples are 0.1 mm (*x*) and 0.15 mm (*y*), which are comparable to those from the calibration samples. The calibration is robust.
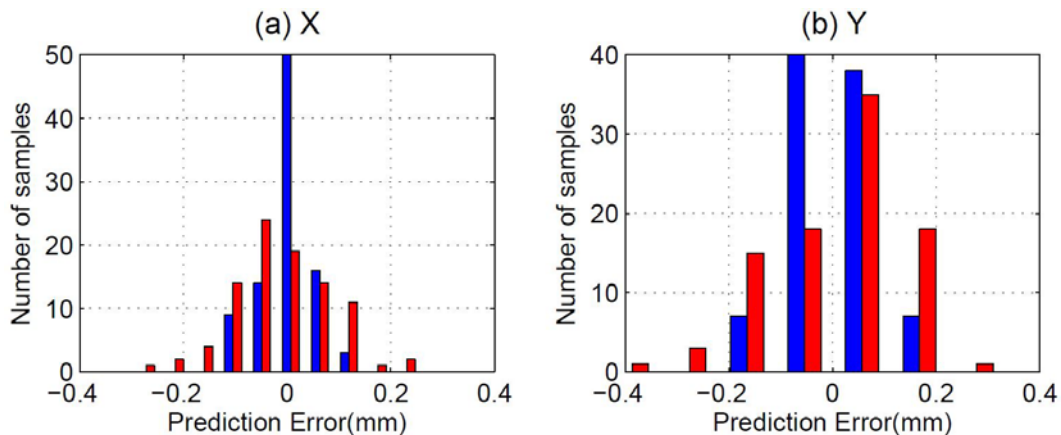
Fig. 23 Difference of measured and predicted transverse beam position from calibration (blue) and validation (red) samples. The method applied is DLR.

The algorithm used in solving the linear system (in the form of Eq. 3) is least squares, which is a standard method to solve linear regression problems. The method relies on minimizing the difference of prediction and measurement of *B* while modifying the elements of the matrix *M*. In our case, the size of matrix *M* is related to the number of sampling points, therefore a considerable number of unknown variables (in our case, 6242) needs to be determined. This is computationally expensive. It is also vulnerable to noise as all sampling points (the entire matrix *A*) are used in the regression. Moreover, even though it is not the case here, overfitting is always a potential problem unless the calibration samples are fairly large. To avoid this risk, it is better to reduce the system size from tens of thousands to several tens, and then apply linear regression on the reduced system. The method we used for this purpose is singular value decomposition.

- **Singular value decomposition (SVD)**

In order to find a small number of prominent components from the spectra matrix, a method known as Singular Value Decomposition (SVD) is used. In general, SVD looks for the patterns of the matrix in terms of SVD modes without the knowledge of any physical parameters (such as dipole mode frequency, quality factor, beam position, etc.). Those SVD modes are natural groupings of the spectra matrix, which are not clearly visible or explicitly defined in the matrix itself.

Applying SVD, the matrix *A* is decomposed into the product of three matrices,

$$A = U \cdot S \cdot V^T \tag{4}$$

where V^T indicates the transpose of *V*. The columns of *U* and V^T are singular vectors of *A*, which form the bases of the decomposition. *S* is a diagonal matrix whose non-zero elements are known as singular values. Applying SVD on the calibration samples, the singular value of each SVD mode is obtained and shown in Fig. 24(a). It can be seen that the first few SVD modes have relatively large singular values; in other words, they are the dominant patterns or natural groupings of the calibration samples. In this case, the first 17 SVD modes are selected for the following analysis.
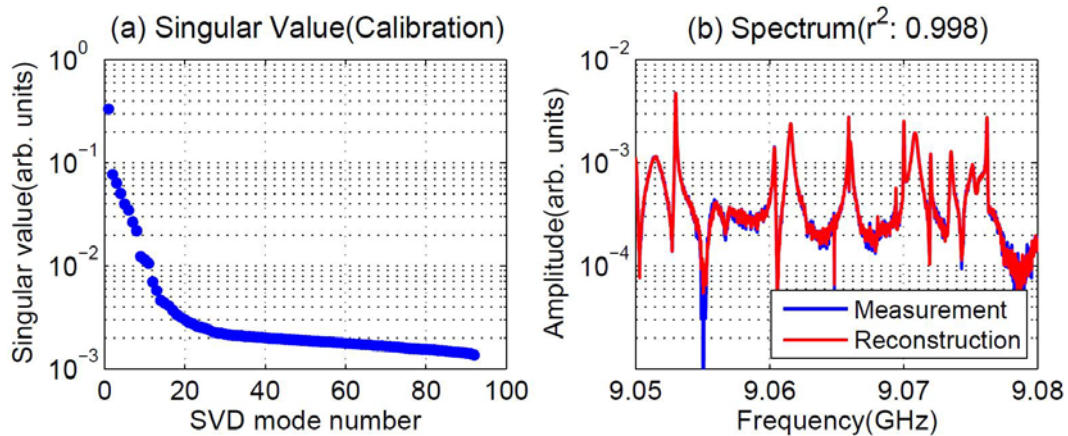
Fig. 24 (a) Singular values of SVD modes; (b) reconstructed spectrum (red) from the first 17 SVD modes compared with original spectrum (blue).

To examine how good the dominant SVD modes are to depict the original spectrum, one can use the first 17 SVD modes to produce an approximation of the spectra matrix *A* as shown in Fig. 24(b). The spectrum can be well represented by using only the first 17 SVD modes.

Having the SVD base vectors from the decomposition, the SVD amplitude can be obtained by

$$A_{SVD} = A \cdot V \tag{5}$$

The size of the matrix *A* is now reduced significantly (18 columns compared to originally 6242 columns). Substituting SVD amplitudes in the regression (Eq. 3), the linear system is now over-determined, which has a well-known best solution. Fig. 25 shows the HOM response from calibration and validation samples by using the first 17 SVD modes to determine the transverse beam position *x* and *y*. The prediction errors remain small and comparable for calibration and validation samples as shown in Fig. 26. The rms error for the validation samples is 0.1 mm for *x* and 0.14 mm for *y*.

HOM ELECTRONICS AND CODE TO
PROBE BEAM CENTRING
ON 3.9 GHZ CAVITIES

Doc. Identifier:
EuCARD-D10 **5 1-report-FINAL-RMJ**

Date: 17/07/2013
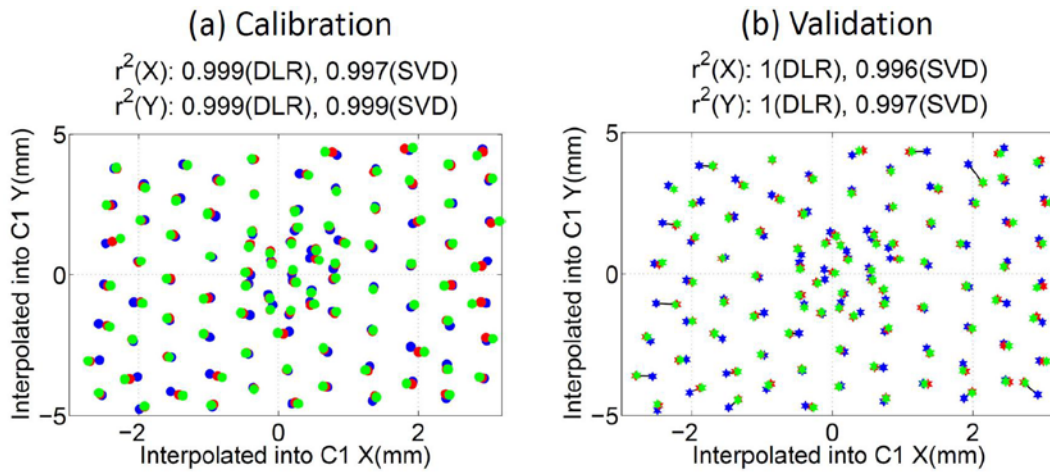
Fig. 25 Measurement (blue) and prediction of the transverse beam position from calibration and validation samples (split as Fig. 20(a)). The method applied is DLR (red) and SVD (green). Points connected with black lines belong to the same beam movement.
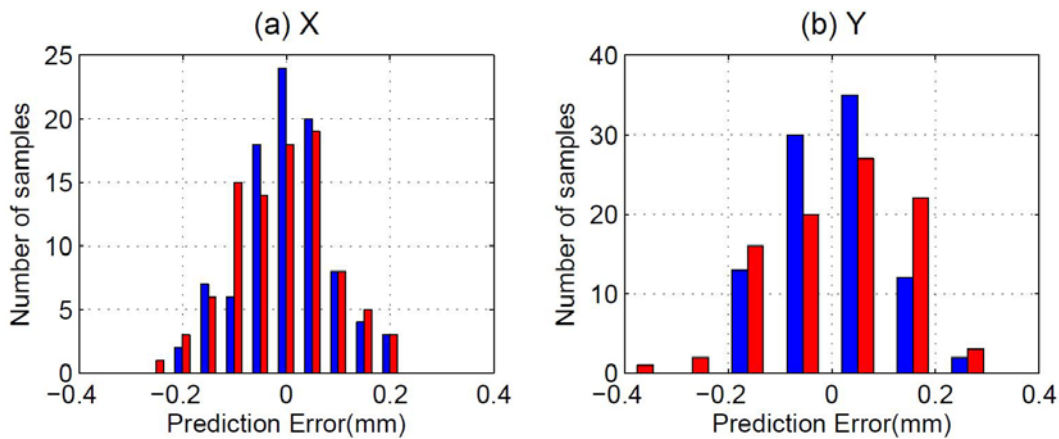
Fig. 26 Difference of measured and predicted transverse beam position from calibration (blue) and validation (red) samples. The method applied is SVD with the first 17 SVD modes.

- **Comparison of DLR and SVD**

A direct comparison of DLR and SVD on the same samples (split as Fig. 20(a)) is shown in Fig. 25. The results are comparable. The comparisons of the prediction errors are listed in Table. 1.

Table. 1 Comparison of rms errors of DLR and SVD for trapped cavity modes in 9.05 - 9.08 GHz and coupled cavity modes in 4.9 - 4.95 GHz.

**HOM ELECTRONICS AND CODE TO
PROBE BEAM CENTRING
ON 3.9 GHZ CAVITIES**

Doc. Identifier:
EuCARD-D10 **5 1-report-FINAL-
RMJ**

Date: 17/07/2013

RMS error	Trapped modes		Coupled modes	
	x(mm)	y(mm)	x(mm)	y(mm)
Calib(DLR)	0.05	0.08	0.06	0.07
Calib(SVD)	0.08	0.09	0.20	0.09
Valid(DLR)	0.10	0.15	0.26	0.32
Valid(SVD)	0.10	0.14	0.24	0.28

In order to improve the prediction accuracy, multiple dipole modes in a narrow frequency band have been used for beam position determination rather than a single dipole mode (two polarizations). Then the number of SVD modes used for regression is determined by the magnitude of the singular values (Fig. 24(a)) and the prediction accuracy from the validation samples. This turns out to be a larger number (17 SVD modes) than that in HOMBPM of TESLA-type cavities (6 SVD modes). This might be due to the fact that modes in the narrow frequency band have individual relationship to the beam scan.

In order to extend the same analysis scheme to all other HOM couplers, spectra from 9.05 GHz to 9.08 GHz are split as Fig. 20(a), then treated with DLR and SVD. The results are shown in Fig. 27. HOM spectra respond well for most couplers but differently to the beam scan for different HOM couplers. This comes from the different spectra and coupling behaviour. It gives rise to special requirements of using HOMs for beam diagnostics, in particular a larger bandwidth is required to capture the frequency shifts among different HOM couplers.

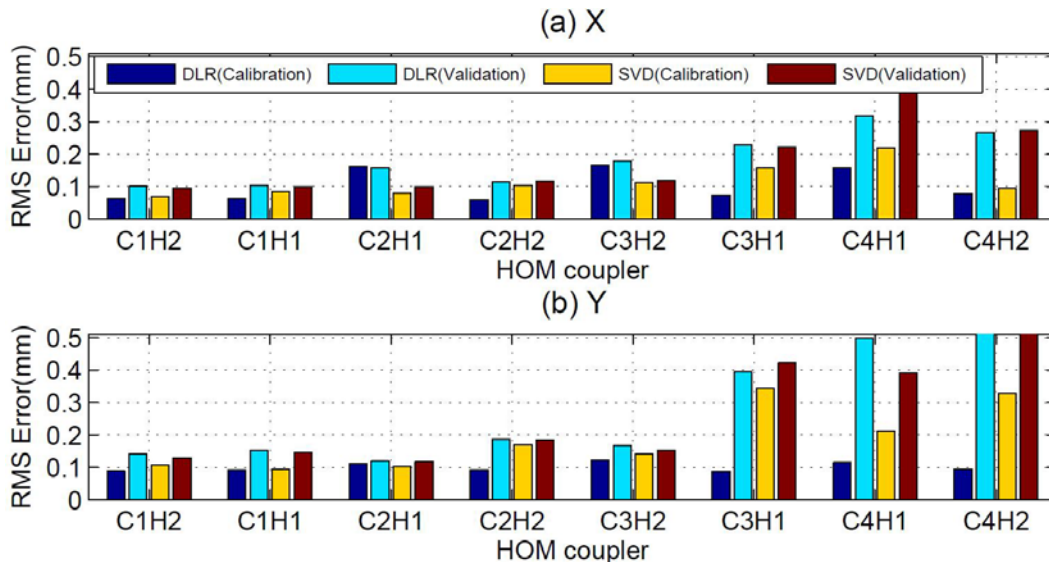*Fig. 27 RMS errors of all eight HOM couplers for spectra between 9.05 GHz and 9.08 GHz and split as Fig. 20(a).*

- **Discussion of the trapped cavity modes**

According to simulations, some modes in the fifth dipole band are trapped cavity modes, meaning that electromagnetic (EM) energy mainly deposits inside each cavity and does not propagate to adjacent cavities through interconnecting beam pipes. This fact enables the beam

position to be determined locally within each cavity. This makes these trapped cavity modes attractive for beam diagnostics compared to the beam-pipe modes, where the EM fields are mainly in the beam pipes and end-cells, and to the first two dipole bands, where the modes couple among cavities. However, modes in the fifth dipole band are located in an upper frequency range, and have small coupling to the beam (small R/Q values). The former will require careful electronics design and the latter will impact the position resolution in the electronics.

3.3.4. Coupled modes in the first two dipole bands

Both transmission and beam-based measurements have indicated a complex HOM spectrum in the third harmonic cavities. Most dipole modes are able to travel from cavity to cavity (see Fig. 10), among which are some strong coupling modes (high R/Q values) in the first two dipole bands. Unlike the localized beam-pipe modes and the trapped cavity modes, these multi-cavity modes enable the transverse beam position to be determined for an entire four-cavity module rather than local position inside each cavity or beam pipe. However, the 3.9 GHz four-cavity string is not significantly longer than one 1.3 GHz TESLA cavity (approximately 1.3 times), the position determined based-on the four-cavity module is still useful. Moreover, position diagnostics on these modes is relevant for beam alignment due to their strong coupling to the beam (high R/Q values).

From simulations, the frequency range from 4.9 GHz to 4.95 GHz covers some strong coupling modes; therefore, the spectra within this 50 MHz bandwidth are used for the following analysis. The beam was moved in a grid manner and split into 32 calibration samples (dots) and 25 validation samples (hexagrams) as shown in Fig. 15(b). Then the positions read from BPM-A and BPM-B are interpolated into the centre of the module.

Similarly, DLR and SVD are applied. The singular values of all SVD modes decomposed from calibration samples are shown in Fig. 28(a). The first ten SVD modes have relatively large singular values, and therefore are used for the following analysis. The measured spectrum is compared with the reconstructed spectrum by using the first ten SVD modes in Fig. 28(b). They possess very good consistency, which indicates the representativeness of the first ten SVD modes in describing the entire signal. The SVD prediction errors for the validation samples are slightly better than those of DLR as shown in Table 1.
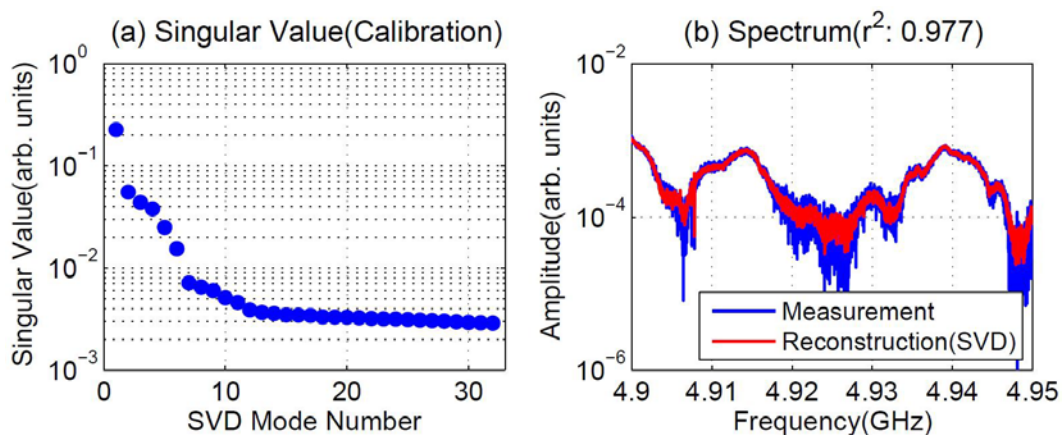

Fig. 28 (a) Singular values of SVD modes; (b) reconstructed spectrum (red) from the first ten SVD modes compared with original spectrum (blue).

**HOM ELECTRONICS AND CODE TO
PROBE BEAM CENTRING
ON 3.9 GHZ CAVITIES**

Doc. Identifier:

EuCARD-D10 **5 1-report-FINAL-
RMJ**

Date: 17/07/2013

Compared to trapped cavity modes (Table 1), coupled modes have larger prediction errors, which is inconsistent with their stronger coupling to the beam (much higher *R/Q*). We believe it is coming from the fact that the signal over noise ratio is better for the trapped cavity modes due to the removal of the 10 dB external attenuator for each coupler during the data taking. This issue will be clarified after the measurements with the electronics.

3.4. SUMMARY OF THE FEASIBILITY STUDY

Beam-excited dipole modes in accelerating cavities can be used to determine beam position and also enables beam alignment to reduce the amplitude of beam-excited higher order modes (HOM). Dependencies of HOMs in third harmonic cavities on transverse beam positions have been observed for the first time. Beam-pipe modes, trapped and propagating cavity modes constitute three options for beam diagnostics. These have been narrowed down and studied by various data analysis techniques. Direct linear regression (DLR) and singular value decomposition (SVD) methods, in particular, have been used to extract beam position from narrow bands of spectra. This is the first time that these two techniques have been compared directly in terms of performance and model complexity in the study of HOM-based beam diagnostics. Predicted beam positions indicate excellent agreement with direct measurements.

Beam-pipe modes and some cavity modes in the fifth dipole band are localized in segments of the module. This enables the beam position to be determined for individual component (beam pipe or cavity). We have identified modes and polarizations of two beam-pipe modes have been observed.

Cavity modes in the first two dipole bands propagate as shown by simulations and measurements. This enables the beam position to be determined for an entire four-cavity module. Good prediction accuracies are achieved with DLR and SVD. Due to their strong coupling to the beam, position diagnostics on these modes is relevant for beam alignment and for a reduction in the amplitude of the wakefield excited.

In this study, rms of the prediction errors is in the order of hundreds of μm for both propagating and trapped modes. They are mainly limited by the resolution of the real-time spectrum analyzer used for the measurement. In order to overcome this limitation, dedicated test electronics for HOM-based beam diagnostics has been built for precise studies and assessment of the modal options.

4. RESOLUTION STUDY WITH THE CUSTOM-BUILT ELECTRONICS

Following the comprehensive series of simulations and HOM measurements of the third harmonic 3.9 GHz cavities described in the previous chapters, we ascertained that there are three significant regions of interest useful for beam position diagnostics. The first region contains modes which are coupled from one cavity to the next within the ACC39 module. The next region is the fifth dipole band containing trapped cavity modes. The third region is the localized dipole beampipe modes. Each region has its own merits. The coupled cavity region, allows a superior position accuracy, whereas the trapped cavity modes or localized beampipe modes allow diagnostics on an individual cavity or beam pipe, but with a reduced accuracy compared to the coupled one. In order to be able to choose the frequency best suited for diagnostics, the three options were studied with the help of a test electronics, which overcomes the resolution limitation of the spectrum analyzer previously used.

Doc. Identifier:

EuCARD-D10 **5 1-report-FINAL-RMJ**

HOM ELECTRONICS AND CODE TO
PROBE BEAM CENTRING
ON 3.9 GHZ CAVITIES

Date: 17/07/2013

In this section, the principle of the test electronics is described in Section 4.1. Trapped cavity modes in the fifth dipole band provide local beam position inside the cavity, and are addressed in Section 4.2. Dimension reduction techniques along with a linear regression have been used to extract the beam position from HOM signals. The dependence of the position resolution on various dipole modes and various time windows is studied. The resolution for a four-cavity-module-based beam position is presented in Section 4.3 using coupled cavity modes in the second dipole band. An analysis of contributors to the position resolutions is presented in Section 4.4.
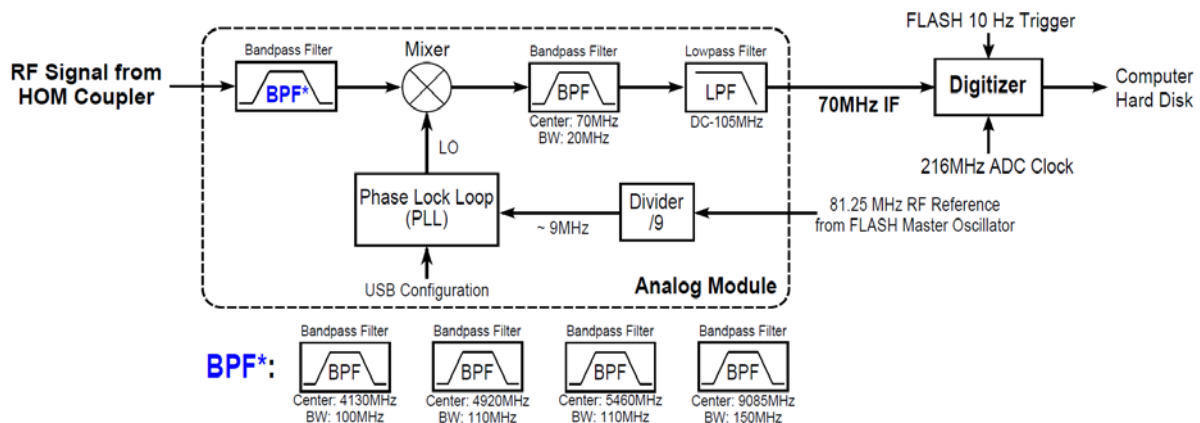
4.1. PRINCIPLE OF THE TEST ELECTRONICS

Fig. 29 Schematics of the HOM electronics. Only one of the four bandpass filters was connected in front of the mixer during each measurement.

A set of test electronics was designed to have the flexibility to study various modal options of interest as well as accommodate the large frequency bandwidths required. Its simplified block diagram is shown in Fig. 29. Each one of the four different analog bandpass filters can be connected into the chain to study localized dipole beam-pipe modes, coupled cavity modes in the first and second dipole band and trapped cavity modes in the fifth dipole band. After filtering, the signal is mixed with a selectable local oscillator (LO) to an intermediate frequency (IF) of approximately 70 MHz. The mixer is a single-side-band mixer with 26 dB image rejection. The LO frequency can be programmed in 9 MHz increments via a USB configuration and retains phase lock with the 9 MHz trigger signal by a Phase Lock Loop (PLL). This 9 MHz trigger is generated by dividing the 81.25 MHz reference signal from the FLASH master oscillator. Then the 70 MHz IF signal is further filtered with a 20 MHz analog bandpass filter to study the specific band of modes. After a lowpass filter, the IF signal has the frequency below 105 MHz with a dominant component from 60 MHz to 80 MHz. The signal is then digitized by a VME digitizer operating at 216 MS/s with 14 bit resolution along with a programmable FPGA for signal processing. The digitizer is triggered by a 10 Hz FLASH machine trigger. Both the selectable LO and the digitizer clock of 216 MHz are locked to the accelerator using signals delivered from the master oscillator as a reference. This locking allows correct phase information of the digitized signal. Digitized data is collected from the digitizer with the EPICS software tool. The beam charge, currents of the steering magnets and BPM readouts are recorded synchronously from the FLASH control system DOOCS. The data processing for position diagnostics is performed offline using MATLAB.

**HOM ELECTRONICS AND CODE TO
PROBE BEAM CENTRING
ON 3.9 GHZ CAVITIES**

Doc. Identifier:

EuCARD-D10 **5 1-report-FINAL-
RMJ**

Date: 17/07/2013

From the measurement results, coupled cavity modes in the second dipole band at approximately 5.44 GHz and trapped cavity modes in the fifth dipole band at approximately 9.06 GHz are promising for beam position diagnostics, and are described in the rest of this section. Example waveforms of the electronics' output when connecting to HOM coupler C3H2 are shown in Fig. 30 for trapped and coupled modes. Each of them is excited by a single electron bunch. HOMs are excited at approximately 100th sampling point, and then decay in a relatively short time.
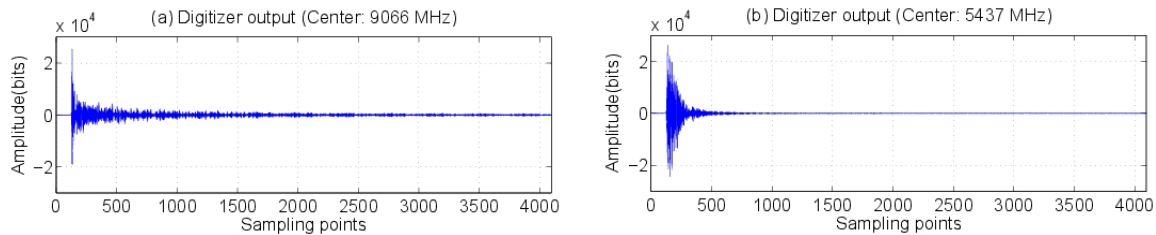

Fig. 30 Signals of the digitizer output for two different bands from HOM coupler C3H2. The length of the waveform is 4096 sampling points corresponding to approximately 19 µs.

4.2. POSITION DIAGNOSTICS WITH TRAPPED CAVITY MODES

In this section, data measured from HOM coupler C3H2 are described. The fourth bandpass filter in Fig. 29 was connected to obtain the fifth dipole band at approximately 9 GHz. The LO has been set to downconvert 9066 MHz to 70 MHz. An example digitizer output is shown in Fig. 30(a).

4.2.1. Data preparation

The frequency components of the waveform in Fig. 30(a) can be obtained by performing a FFT (Fast Fourier Transform). The magnitudes of these signals are shown in Fig. 31(a). From previous studies, we know that modes below the double peaks at approximately 55 MHz are propagating amongst cavities, therefore an ideal filter has been applied mathematically on the waveform to cut away the frequency components below 58 MHz and above 96 MHz. Only the region within the two dash lines in Fig. 31(a) has been preserved. Since the signal decays very fast (see Fig. 30(a)), a time window has been applied on the filtered waveform to reduce the signal length. The final waveform has a length of 700 sampling points (corresponding to approximately 3.2 µs) as shown in Fig. 31(b), and will be used in the following study.
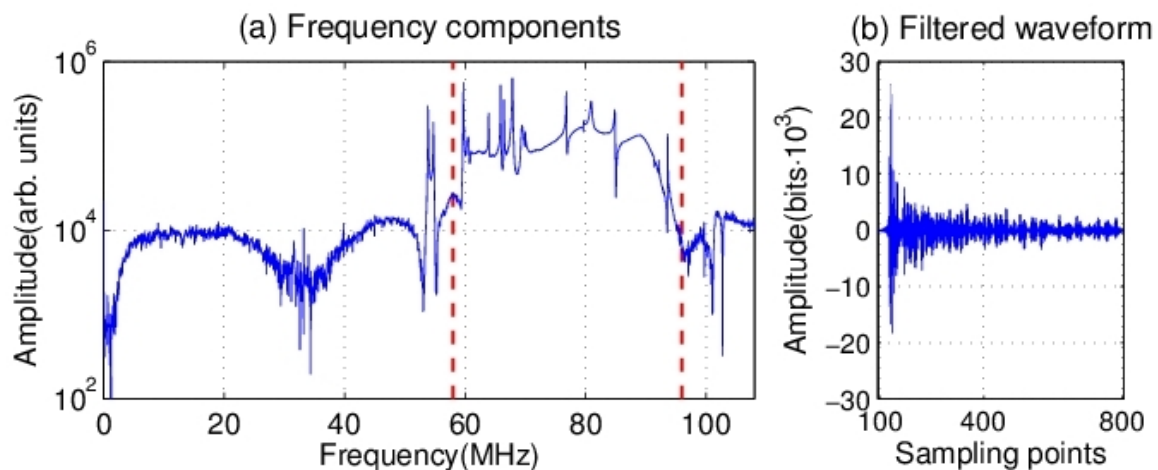
Fig. 31 Frequency components of the digitized signal and a time-domain waveform after applying the ideal filter and a time window.

The beam has been moved in a 2D-grid manner by using steering magnets located upstream of the ACC1 module as shown in Fig. 14. We have switched off the non-linear elements from the RF gun up to BPM-B, i.e. the quadrupole magnets and the RF of ACC39 and removed the dark current collimator so as to create a straight-line beam trajectory. The RF of ACC1 was left on due to difficulties to transport the beam at 5 MeV. This however induces significant technical difficulties to move the beam in a random angle. Two BPMs have been used to record the transverse beam position before and after the bunch entering ACC39. These are BPM-A and BPM-B as shown in Fig. 14. The FLASH machine was operated in single bunch mode with a bunch charge of approximately 0.5 nC. A toroid situated right after BPM-B was used to record the bunch charge. A position interpolation is applied to obtain the transverse beam position in each cavity as shown in Fig. 32 for C3 as an example. These interpolated positions are used in the following study. We first took 49 calibration samples (blue dots in Fig. 32) and then 36 validation samples (red dots in Fig. 32).
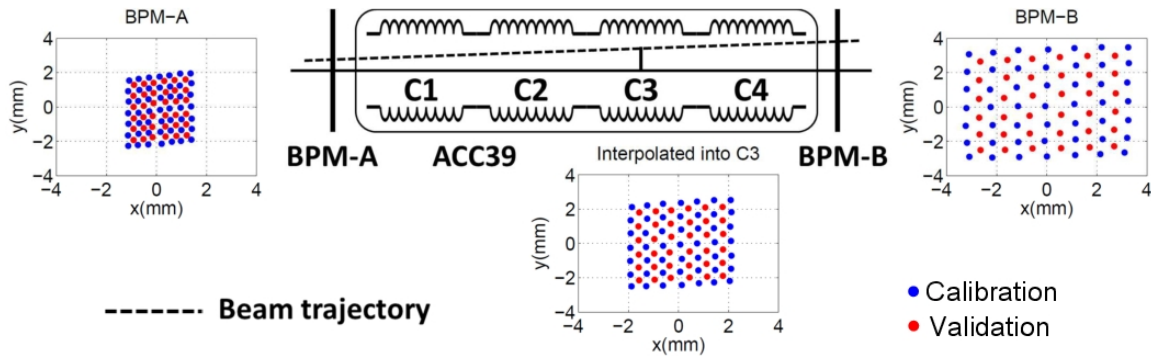

Fig. 32 Position interpolated into the center of C3 from the readouts of BMP-A and BPM-B.

4.2.2. Extract beam position from HOM waveforms

Having the HOM waveforms and the interpolated beam positions, a linear regression is used to determine their correlations. Prior to the linear regression, a singular value decomposition (SVD) method is applied on the HOM waveforms. This is used to reduce the dimension of the linear system and suppress noises present in the HOM waveforms. The first twelve SVD modes have relatively large singular values, therefore their SVD mode amplitudes are used to regress on the interpolated beam positions instead of the original HOM waveforms. A calibration of the HOM signals is generated in this manner. The predictions of beam position are made by applying the calibration on the validation samples. These predictions are then compared with the measured position interpolated into the cavity. The rms of the position residuals (rms error) is defined as the position resolution.

Focusing on analysis using the first twelve SVD modes, predictions of beam position are obtained and compared with the measured beam position as shown in Fig. 33(a). A coefficient of determination r2 is calculated to characterize the overall prediction errors. The residuals are shown in Fig. 33(b) and Fig. 33(c). From this we ascertain a position resolution of 45 μm for *x* and 54 μm for *y*.
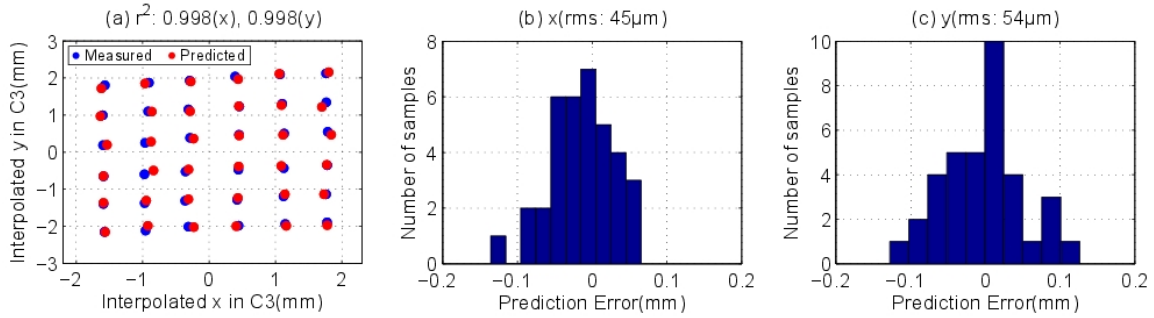
Fig. 33 Prediction of the transverse beam position using the first twelve SVD modes. (a) Measurement is in blue and prediction is in red. Points connected with black lines belong to the same beam position. (b)(c) Prediction errors of x and y. The position resolution is denoted as the rms value.

4.2.3. The search for suitable dipole modes

Detailed simulations have shown that modes in the fifth dipole band have small R/Q's, and therefore couple weakly to the beam. This will affect the resolution of beam position in the cavity measured with these dipole modes. In order to improve the resolution, we use a band of modes for position determination as shown in the previous section. This is different from the previous study, which uses two polarizations of one dipole mode. In Fig. 34(a), the resolutions for x and y using a band of modes are shown as the long magenta lines on the bottom. These are compared with resolutions using different segments of the band. The colour of the segment in Fig. 34(b) matches the colour of the resolution lines in Fig. 34(a). An ideal filter is applied mathematically on the time-domain digitizer output (Fig. 30(a)) using the bandwidth of each segment in Fig. 34(b). A time window is then applied on the filtered waveform to truncate the signal properly. Fig. 34(a) reveals a remarkable improvement in the resolution achieved through combining modes in the trapped band.
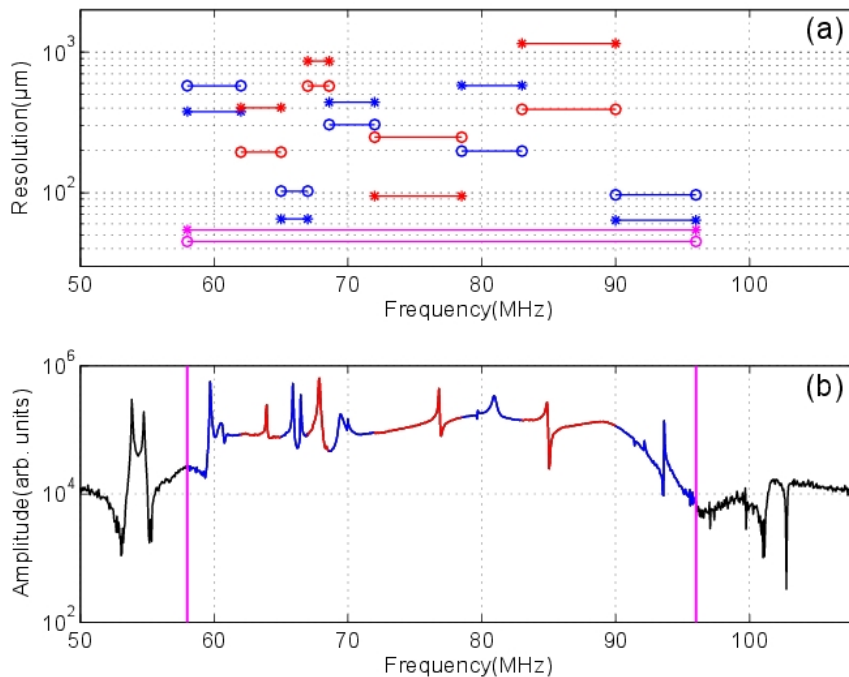

Fig. 34 Resolutions of each segment of spectrum. Circles denote x and asterisks denote y.

Due to a smaller size of the third harmonic 3.9 GHz cavity compared to the TESLA 1.3 GHz cavity, the eigenmodes of ACC39 are particularly sensitive to small geometrical errors. Predicting the exact frequency locations of these modes is impractical. This is another reason to utilize the signal of a complete band of frequencies to accommodate the frequency shifts of dipole modes extracted from different cavities.

4.2.4. The search for a suitable time window

HOMs in the fifth dipole band decay rapidly as shown in Fig. 30(a). In this section, we study the resolution dependence on the time window applied on the waveforms. Starting from the 100th sampling point, the length of the time window increases in the forward direction by a step of 50 sampling points. This is illustrated in Fig. 35(a). The waveforms with each time window are then treated with SVD and various number of SVD modes are subsequently used for position determination. The resolutions are shown in Fig. 35(b) and Fig. 35(c) for different time window and different number of SVD modes. In Fig. 35(b), a minimum length of time window starting from the 100th and ending at the 300th sampling point with eleven SVD modes gives a reasonably good resolution of 47 μm for *x*. The same time window with nine SVD modes suggests a resolution of 49 μm for *y* as shown in Fig. 35(c).
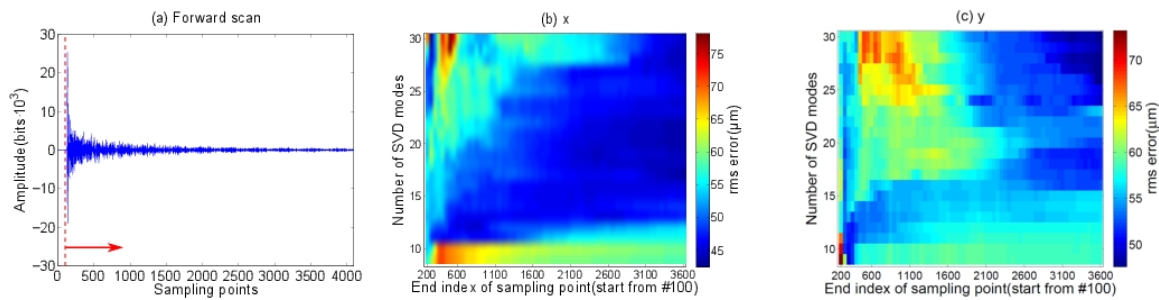
Fig. 35 Scan forward starting from the 100th sampling point.

Having found the smallest end index, the 300th, of the time window from the forward scan, we conduct a backward scan by moving the start index of the sampling point in the backward direction with a step of 10 sampling points. This is shown in Fig. 36(a). A shorter time window from the 140th to the 300th with eleven SVD modes give a same resolution of 47 μm for *x* as shown in Fig. 36(b). A resolution of 51 μm for *y* is expected by using the same time window with nine SVD modes as shown in Fig. 36(c).

Fig. 36 Scan backward ending at the 300th sampling point.

The findings from the forward and backward scans are summarized in Table 2. The length of the time window is also calculated in terms of time. As a comparison, the resolutions with the time window used in the previous section are also listed. In an extreme case, the full length of

the waveforms is also treated in the same way and resolutions are calculated. From the table, we conclude that a small length of waveform contains enough information to dete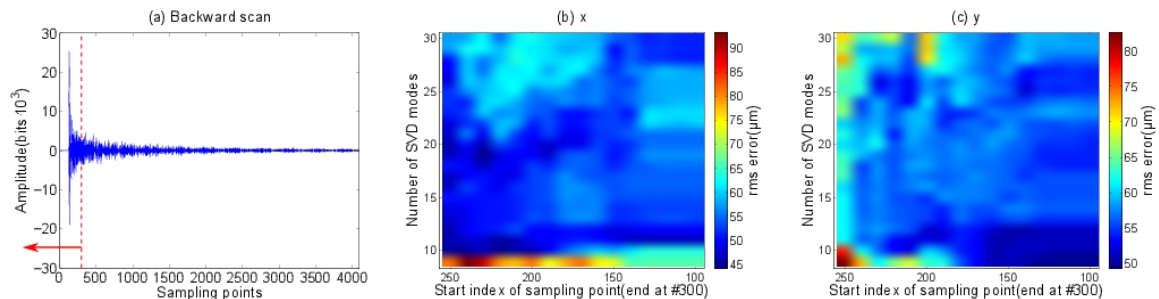rmine beam position with reasonably good resolution. The first 40 sampling points (from the 100th to 140th, corresponding to approximately 0.19 μs) which have large amplitude appear to be insensitive to beam movement. This might be due to a beam pulse effect.

Table 2: Resolution of various segments of waveform with different number of sampling points.

	Sampling points			Resolution		SVD modes	
	start index	end index	time (μs)	x (μm)	y (μm)	x	y
Forward scan	100	300	0.9	47	49	1st–11th	1st–9th
Backward scan	140	300	0.7	47	51	1st–11th	1st–9th
Full segment	100	800	3.2	45	54	1st–12th	1st–12th
Full waveform	1	4096	18.9	43	45	1st–17th	1st–25th

As shown in Table 2, the backward scan suggests a time window from 140th to 300th with a length of 0.7 μs. This length is shorter than the bunch separation of 1 μs at FLASH when operated in a multi-bunch mode. Fig. 37 shows the waveform with different time windows. The black lines represent the multiple bunches separated by 1 μs, while the red dash lines define the shortest time window found with reasonably good position resolution. This suggests non-degenerate position resolutions of the leading bunch in a bunch train. Although HOMs seem to decay fast, there is still a remaining signal from the current bunch overlapping with HOMs excited by the trailing bunches. This will dilute the beam position resolution of bunches following the leading bunch in a train at FLASH. However, degenerate beam positions of trailing bunches are also useful.
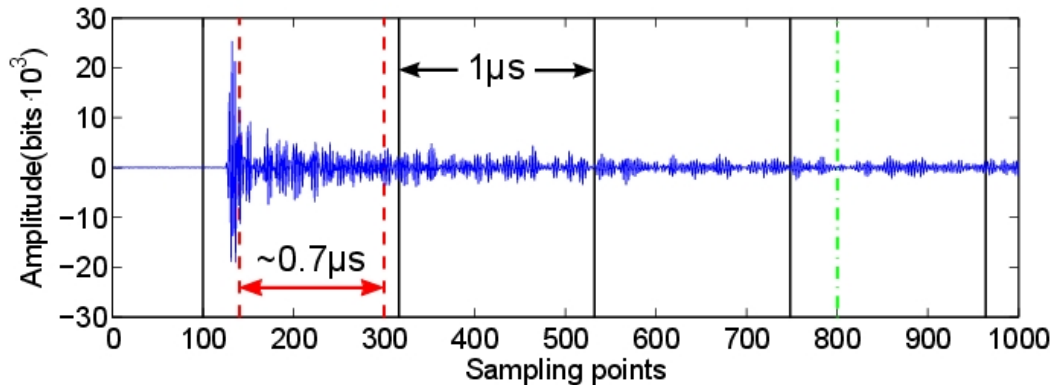
Fig. 37 Waveform with various time window.

4.3. POSITION DIAGNOSTICS BASED ON A BAND OF COUPLED CAVITY MODES

Previous studies have shown that modes in the first two dipole bands propagate amongst all cavities within the ACC39 module. This enables the beam position to be determined in a four-cavity-module sense rather than an individual cavity. Therefore, we interpolate the two BPM readouts into the centre of the module and study the beam position resolutions at this location. Simulations predict some strong coupling modes (with large R/Q values) in the first two dipole bands. HOM BPMs using these modes will potentially have higher resolutions. In this section, modes in the second dipole band measured from HOM coupler C3H2 are used. The

third bandpass filter in Fig. 29 was connected. The LO has been set to downconvert 5437 MHz to 70 MHz. An example digitizer output is shown in Fig. 30(b). The frequency components obtained by a FFT are shown in Fig. 38(a). A time window has been applied to cut away the saturated part of the waveform at the beginning of the signal (cut at the 170th sampling point), as well as the trailing part due to a fast signal decay (end at the 500th sampling point). The resulting waveform is shown in Fig. 38(b). These waveform slices are used to determine the beam position at the centre of the module.
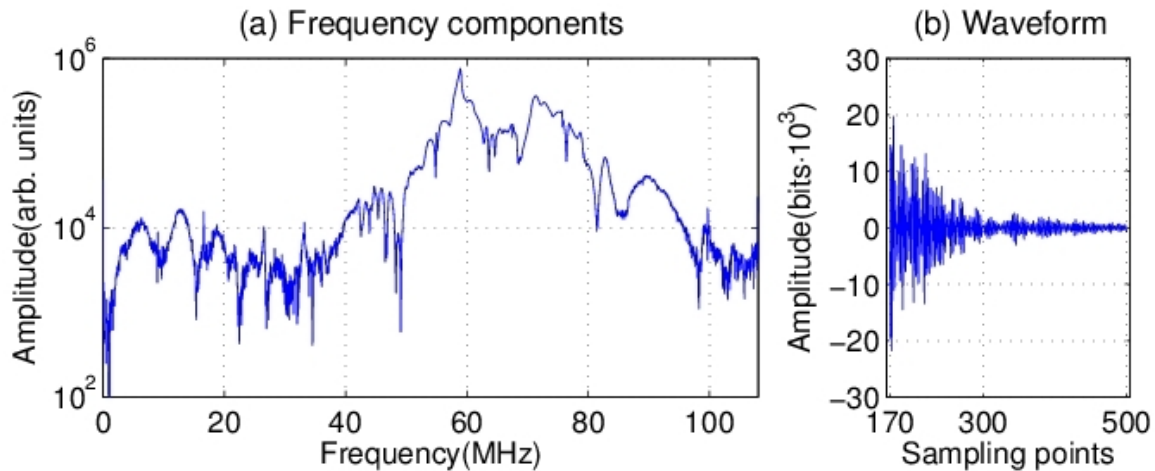

Fig. 38 Frequency components of the digitized signal and a waveform slice after applying a time window.

Using the first eleven SVD modes, the predicted positions are compared with measured ones as shown in Fig. 39(a). Excellent consistency can be observed. The position resolution is 20 μm for *x* and 23 μm for *y* as shown in Fig. 39(b) and Fig. 39(c).
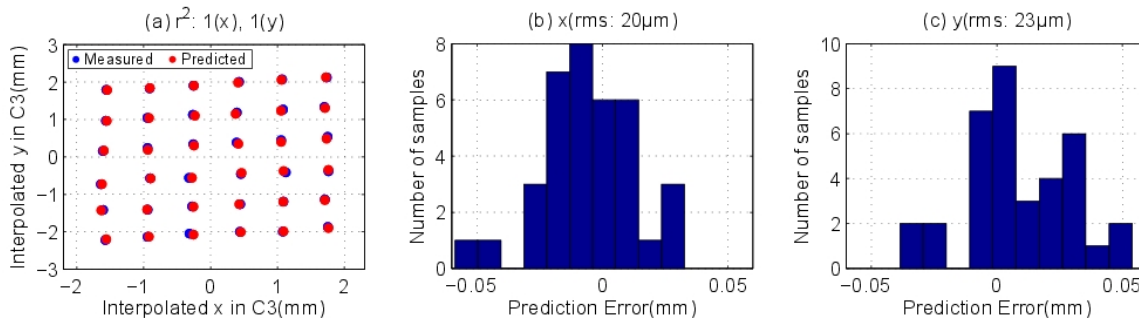
Fig. 39 Prediction of the transverse beam position using the first eleven SVD modes. (a) Measurement is in blue and prediction is in red. Points connected with black lines belong to the same beam position. (b)(c) Prediction errors of x and y. The position resolution is denoted as the rms value.

To study the electromagnetic energy distribution of these coupled modes, the HOM power is integrated over a frequency range from 1 MHz to 107 MHz (see Fig. 38(a)) for each beam position. The power distribution of these coupled modes extracted from each HOM coupler is shown in Fig. 40. A similar position with minimum power can be found from all eight couplers although the exact distribution for each coupler is dissimilar. This might be due to different orientations of the couplers as shown in Fig. 3(b) and different types, therefore individual coupling to the HOMs. The longitudinal electromagnetic field distribution of these coupled modes can also contribute. Around this common position with minimum HOM power, a smaller scan was conducted as shown in Fig. 41(a). The resolution of predicting the

transverse beam position at the centre of the four-cavity module is obtained by using the HOM signal extracted from each of the eight couplers. This is shown in Fig. 41(b). Our study predicts a resolution of 10 – 25 μm for *x* and 20 – 30 μm for *y*.
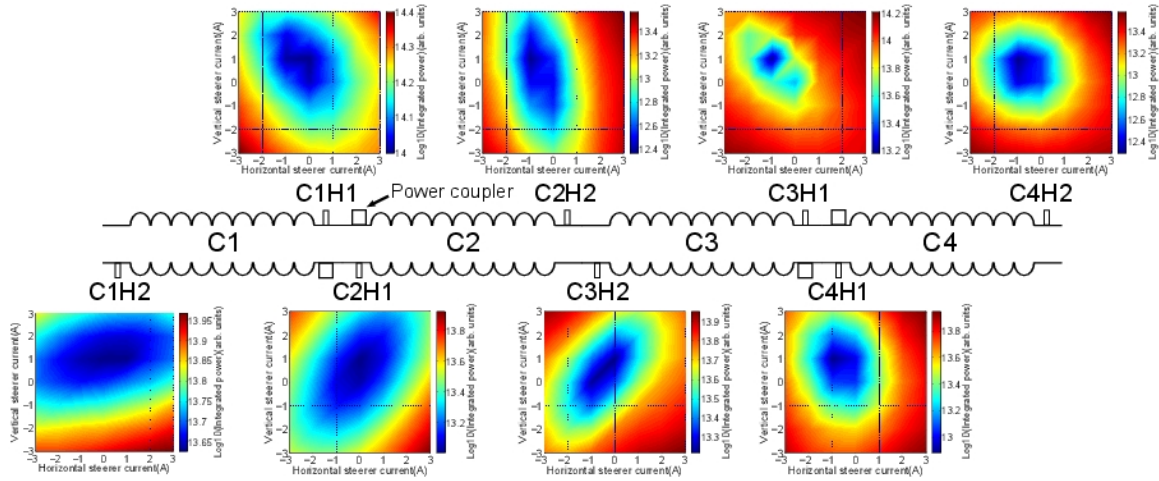
Fig. 40 Integrated power (log scale) as a function of steering magnets' current.
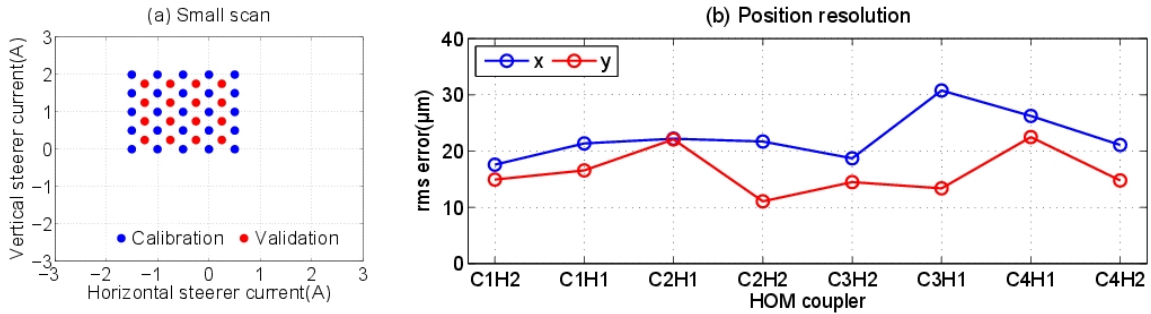
Fig. 41 Small scan (a) and the corresponding position resolution for each coupler (b).

4.4. FUNDAMENTAL LIMITATIONS TO POSITION RESOLUTION

The position resolution presented in previous sections receives contributions from many factors, which are estimated in this section. Fundamentally, the measurement resolution is limited by thermal noise, which is of course unavoidable at a non-zero temperature. The smallest measurable thermal energy, U_{th}, is

$$U_{th} = \frac{1}{2} k_B T \qquad (6)$$

where *T* is the temperature and k_B is the Boltzmann constant (8.6×10^{-5} eV/K). Assuming a room temperature of 300 K, $U_{th} = 0.0129$ eV.

A beam with charge *q* traversing a cavity loses an energy *U* in a particular mode as

$$U = \frac{\omega}{2} \cdot \left(\frac{R}{Q}\right) \cdot q^2 \qquad (7)$$

where *R/Q* has the unit of Ω/cm² for dipole modes. A fraction, *β*, of this energy radiates to the HOM coupler, where we use 0.5.

EuCARD

Doc. Identifier:

EuCARD-D10 **5 1-report-FINAL-RMJ**

HOM ELECTRONICS AND CODE TO
PROBE BEAM CENTRING
ON 3.9 GHZ CAVITIES

Date: 17/07/2013

For the third harmonic 3.9 GHz cavity, the modes with the strongest coupling in the second dipole band has a simulated frequency of 5.4427 GHz and an *R/Q* value of 20.877 Ω/cm^2. The energy deposited in the cavity from a 1 nC beam is

$$U = \beta \cdot \frac{\omega}{2} \cdot \left(\frac{R}{Q}\right) \cdot q^2 = 1.1 \times 10^{12} \, eV \cdot cm^{-2} \tag{8}$$

This corresponds to a transverse beam offset

$$r = \sqrt{\frac{U_{th}}{U}} = 1nm \tag{9}$$

HOM signals are brought from the coupler inside the FLASH tunnel to the HOM patch panel outside the tunnel by long cables. The measured cable loss is approximately 20 dB, the electronics attenuation is 26 dB, and this degrades the resolution by a factor of f_{cable} as

$$r^* = f_{cable} \cdot r = 10^{\frac{20dB+26dB}{20}} \cdot r = 200nm \tag{10}$$

The theoretical minimum resolution is therefore 200 nm, as compared to the observed resolution of 10 – 30 μm (see Fig. 41). This discrepancy may be due to four main issues.

First, HOM signals are all normalized to the bunch charge before the position prediction. The bunch charge was recorded from the nearby toroid, which has a measured resolution of 3 pC (rms). The measured bunch charge was approximately 0.5 nC throughout our studies, therefore it corresponds to a relative resolution of ~0.6%. At 1 mm beam offset, this contributes ~6 μm to the position resolution.

Second, readouts of two BPMs are used to interpolate the beam position into the cavity/module and then to calibrate the HOM signals. These two BPMs have a measured resolution of ~10 μm (rms), contributing to the resolution of the HOM-based system.

Third, the phase noise of the LO used to down-mix the HOM signal can also contribute to the resolution. This need to be studied in future measurements.

Fourth, the resolution we have obtained is in a global sense, since the rms is calculated on the prediction errors for all different beam offsets. Only one prediction is made for each individual beam position. This is a characterization of the prediction power for the entire beam scan, which is not usually used in beam diagnostics where resolution is quoted for a specific beam position. In this case, the position varies mainly due to beam jitter from bunch to bunch. Initial studies on measuring beam jitter for specific beam offsets suggest improved resolutions by at least a factor of 2.

Therefore, it can be seen that the measured position resolution is dominated by the BPM resolution used for position interpolation. For the measurement of local position inside each cavity, BPMs can be used to calibrate HOM signals in C1 and C3, the position measured in these two cavities can then be used to make a prediction about the position in C2. In this case, the limitations of BPMs are eliminated from the position prediction in C2, and might consequently improve the resolution.

4.5. SUMMARY OF THE RESOLUTION STUDIES

The modes within the ACC39 third harmonic accelerating module fall into two distinct categories: trapped modes and coupled inter-cavity modes. A detailed study based on

experiments at the FLASH facility has been conducted in order to assess their relative merits and potential resolution. We have studied various modal options with a set of test electronics. Based on the measurement results, one band for each category appears to be promising for beam position diagnostics. The trapped cavity modes are used to determine the individual beam position in each cavity, and the resolution is approximately 50 μm. The transverse beam position at the centre of the accelerating module can be determined by using the coupled modes, and the resolution is approximately 20 μm due to the strong coupling of these modes to the beam. A set of dedicated electronics is being built using modes in the second dipole band and the fifth dipole band, in order to facilitate high resolution measurements for the whole module, and reasonable resolution for localized measurements within individual cavities. Based on the results of this study, we anticipate providing similar HOM diagnostics for the European XFEL third harmonic module consisting of eight cavities.

5. STATISTICAL METHODS FOR BEAM POSITION EXTRACTION

Beam position information is concealed in HOMs. Signals are well defined in conventional BPMs, thus the beam position can be determined in a straightforward way. However, HOMs in third harmonic 3.9 GHz cavities are much more complex as discussed in previous sections, therefore advanced data analysis methods are required in order to extract the beam position information from HOMs effectively.

In order to extract beam position information, linear regression can be used. Due to a large number of sampling points in the waveforms, statistical methods are used to effectively reduce the dimension of the system, such as singular value decomposition (SVD) and *k*-means clustering. These are compared with the direct linear regression (DLR) on the entire waveforms. A cross-validation technique is used to study the sample independent precisions of the position predictions given by these three methods. A RMS prediction error in the beam position of approximately 50 μm can be achieved by DLR and SVD, while *k*-means clustering suggests 70 μm.

5.1. ALGORITHMS FOR BEAM POSITION DIAGNOSTICS

The test electronics have been connected to the upstream HOM coupler of C3 as shown in Fig. 2. The digitized data has been filtered such that only the trapped cavity modes in the fifth dipole band from 9040 MHz to 9078 MHz are preserved and then normalized to the beam charge. These modes are of particular interest since they can provide localized beam position information. We have steered the beam in a two-dimensional grid manner by using a pair of steerer magnets located upstream of ACC39 module as shown in Fig. 14. The RF of ACC39 and the nearby quadrupole magnets were both switched off in order to produce a straight-line beam trajectory between the two beam position monitors: BPM-A and BPM-B. Thus the transverse beam positions inside the cavity can be determined from the readouts of the two BPMs by linear interpolation. The detailed setup of the FLASH machine for this study can be found in Section 2.1. The goal is to extract transverse beam position from the HOM waveforms.

5.1.1. Data preparation

The HOM waveforms for 85 different beam positions are shown in Fig. 42(a). The corresponding beam positions are shown in Fig. 42(b) (blue and red dots).
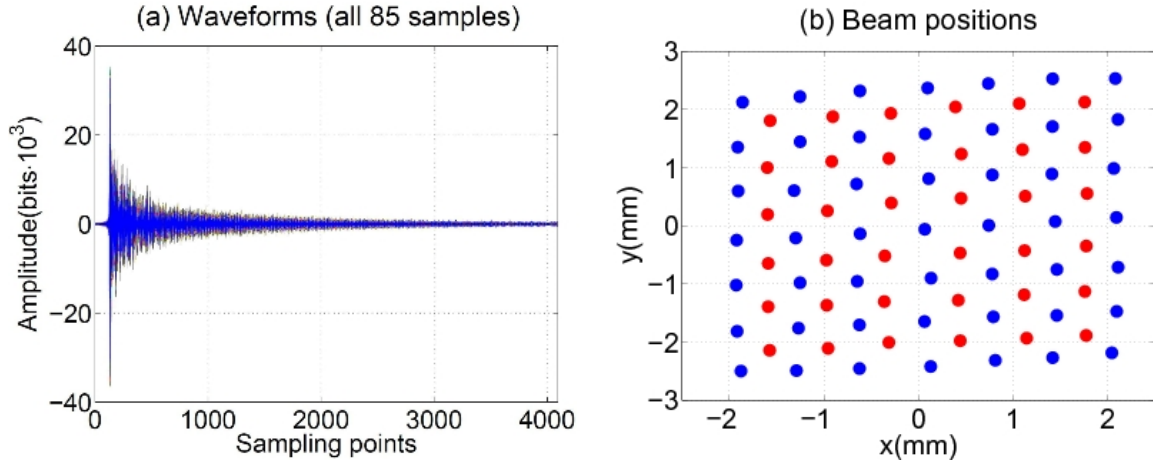
HOM ELECTRONICS AND CODE TO
PROBE BEAM CENTRING
ON 3.9 GHZ CAVITIES

Doc. Identifier:

EuCARD-D10 **5 1-report-FINAL-RMJ**

Date: 17/07/2013

Fig. 42 (a) Waveforms of all 85 samples. (b) Fixed sample split. Calibration samples are in blue and validation samples are in red.

In order to define the problem, we arrange the waveforms and beam positions in matrix forms. The matrix *A* contains the waveforms and is constructed as

$$A = \begin{pmatrix} waveform_1 \\ waveform_2 \\ \vdots \\ waveform_m \end{pmatrix} = (a_1, a_2, \ldots, a_n) \in \mathbb{R}^{m \times n}.$$

(11)

A is a *m×n* matrix. $a_i \in R^m$ is the ith column of *A*, which contains values of the ith sampling point from all *m* waveforms. Each waveform has 4096 sampling points, therefore n = 4096.

The matrix *B* contains the interpolated beam positions and is constructed as

$$B = \begin{pmatrix} x_1 & y_1 \\ x_2 & y_2 \\ \vdots & \vdots \\ x_m & y_m \end{pmatrix} \in \mathbb{R}^{m \times 2}.$$

(12)

B is a *m×2* matrix. x_i and y_i are the ith transverse beam positions at the centre of the cavity corresponding to the measurement of *waveform_i*. There are technical difficulties which would be entailed in obtaining angle effects in ACC39 independently. As the contribution of the angle wakefield is much smaller than that of the offset wakefield, the angle is not considered in this study.

Now we have built a system consisting of waveforms *A* and beam positions *B*. To study this system, we split the samples in a fixed manner as shown in Fig. 42(b). 49 samples are used for calibration (blue) and the remaining 36 samples for validation (red). Therefore, calibration samples have *m* = 49 and validation samples have *m* = 36 in both Eq. 11 and Eq. 12.

5.1.2. Direct linear regression

To extract beam position information from the waveforms, a straightforward method is Direct Linear Regression (DLR),

$$A \cdot M = B$$

(13)

where $A \in R^{m \times (n+1)}$ with one column of 1 added to the waveform matrix defined in Eq. 11 representing the intercept term, $B \in R^{m \times 2}$ is the position matrix defined in Eq. 12,

HOM ELECTRONICS AND CODE TO
PROBE BEAM CENTRING
ON 3.9 GHZ CAVITIES

Doc. Identifier:

EuCARD-D10 **5 1-report-FINAL-
RMJ**

Date: 17/07/2013

$M \in R^{(n+1)\times 2}$ is the matrix of regression coefficients. M is further represented as $(M1, M2)$, where M_k is a $(n + 1)\times 1$ vector ($k = 1$ or 2). The matrix M is obtained by solving the linear system composed by matrix A and B.

The linear system is highly under-determined where m n, which is vulnerable to overfitting. Therefore, we used a modified least square algorithm to do the linear regression: Regularized Least Squares (RLS). A regularization term is added into the normal error function in order to control the overfitting. The RLS error function is therefore defined as

$$J_k = \frac{1}{2}\sum_{i=1}^{m}(B_i^{pre}-B_i)^2 + \frac{\lambda}{2}\|\overrightarrow{M_k}\|^2 \quad (k=1,2)$$

(14)

where B_i^{pre} is the predicted beam position calculated by using Eq. 13, B_i^{pre} and B_i represent x when $k = 1$ or y when $k = 2$, $\|\vec{M}_k\|$ is the 2-norm of M_k, and λ is the regularization coefficient controlling the relative importance of the regularization term. λ provides a shrinkage of the value of the regression coefficients in M. The linear regression is therefore performed by minimizing the RLS error functions while updating the elements of M. A figure of merit has also been defined in order to evaluate the goodness of the regression: the root-mean-square (RMS) error,

$$E_{RMS} = \sqrt{\frac{1}{m}\sum_{i=1}^{m}(B_i^{pre}-B_i)^2}.$$

(15)

E_{RMS} has the unit of *mm*, which is the same as B_i^{pre} and B_i.

The impact of the regularization term in Eq. 14 on the prediction error can be seen in Fig. 43 by plotting the RMS errors of both calibration and validation samples against the regularization coefficient λ. A model with a $\lambda < 10^8$ has a stable and promising performance, while in contrast a poor fit emerges for a large λ. The complexity of the model is now controlled with λ overseeing the degree of overfitting. When $\lambda < 10^7$, the RMS errors fall sharply for calibration samples while slightly rise for validation samples. This is an indication of overfitting due to the lack of control by a too small λ. Thus we choose $\lambda = 10^7$ for the following analysis.
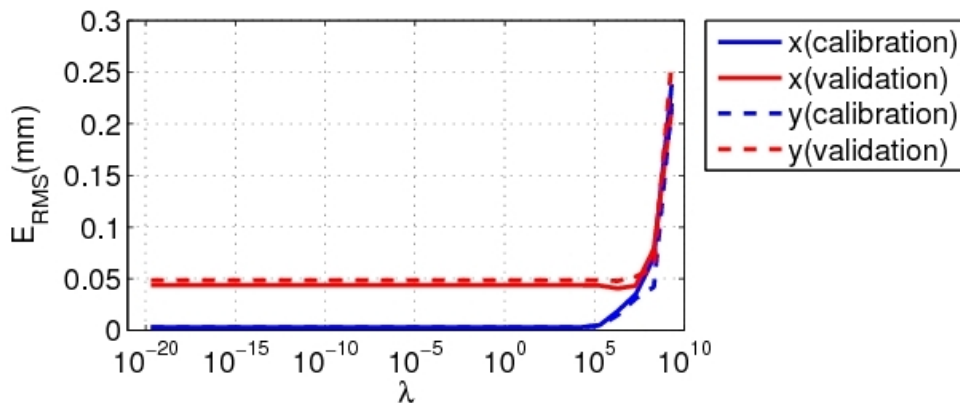

Fig. 43 RMS error versus λ.

HOM ELECTRONICS AND CODE TO PROBE BEAM CENTRING ON 3.9 GHZ CAVITIES

The value of the RLS error function is reduced in each iteration while performing the linear regression as shown in Fig. 44(a). The difference of the J's between two consecutive iterations is denoted as ΔJ. The values of J's decrease evidently when $\Delta J > 10^{-7}$, and then land on a relatively flat region between 10^{-9} and 10^{-7} of ΔJ. The RMS errors of both calibration and validation samples for each iteration are shown in Fig. 44(b). The prediction power on the validation samples stabilizes after $\Delta J < 10^{-6}$. An overfitting emerges while $\Delta J < 10^{-7}$ as the RMS errors of calibration samples drop sharply, while the RMS errors of validation samples rise slightly. Therefore, we set that the calculation stops when $\Delta J < 10^{-7}$.
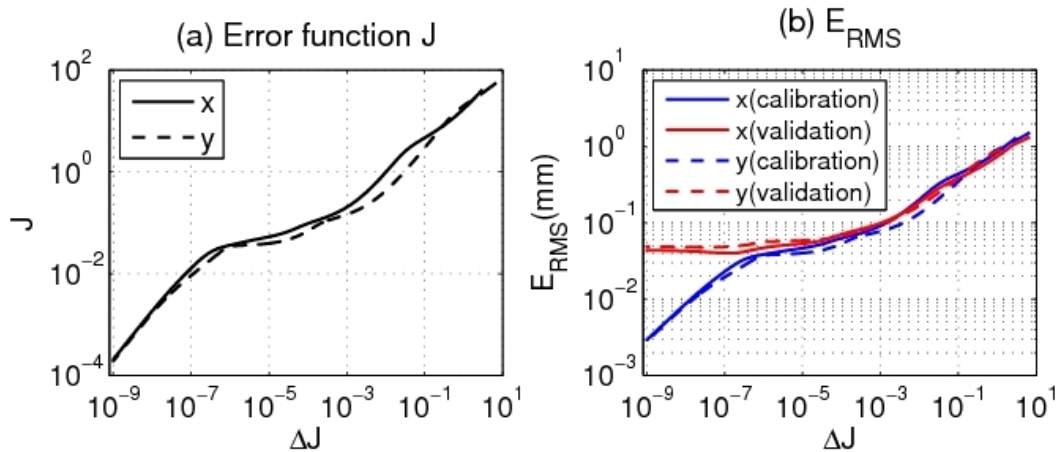

Fig. 44 Error function and RMS error in calculating the calibration matrix M.

Using $\lambda = 10^7$ and $\Delta J < 10^{-7}$, the predicted beam positions are obtained by RLS and then plotted together with the direct measurement for both calibration and validation samples in Fig. 45. To measure the consistency, the coefficient of determination r^2 is calculated. The differences between predicted and measured positions are shown in Fig. 46 as the residuals. The RMS error on the validation samples is 40 μm for x and 50 μm for y.
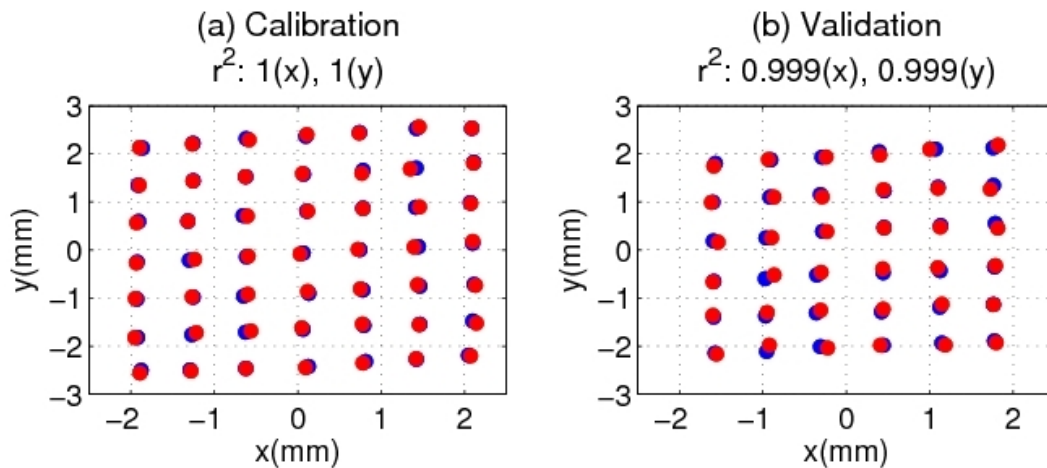

Fig. 45 Measurement (blue) and prediction (red) of the transverse beam position from calibration and validation samples. The method applied is DLR.
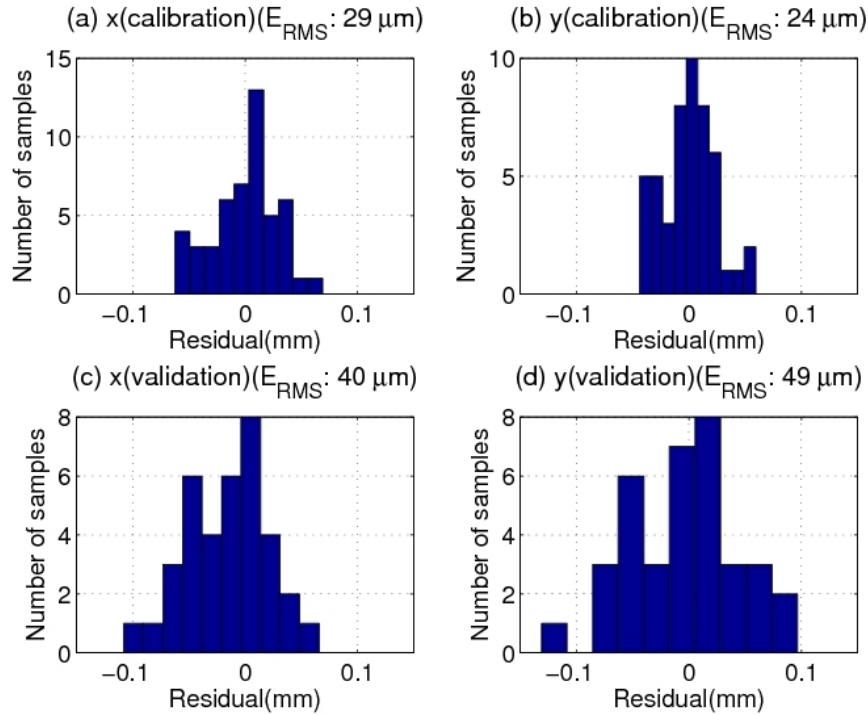
Fig. 46 Difference of measured and predicted transverse beam position from calibration and validation samples. The method applied is DLR.

The size of matrix M is 4097×2. A considerable number of unknown variables need to be determined. This is computationally expensive. As all sampling points are used in the regression, each column of matrix A, a_i, is a regressor. The correlation coefficients $R(i, j)$ of these regressors are calculated as

$$R(i,j) = \frac{\mathrm{Cov}(a_i,a_j)}{\sqrt{\mathrm{Cov}(a_i,a_i) \cdot \mathrm{Cov}(a_j,a_j)}}$$

(16)

where a_i and a_j are i^{th} and j^{th} column of matrix A as defined in Eq. 11, $\mathrm{Cov}(a_i, a_j)$ is the covariance between two regressors a_i and a_j. In this definition, $R = \pm 1$ corresponds to a strong correlation while $R = 0$ indicates no correlation at all. Fig. 47 shows the correlation coefficients of the calibration samples. Most regressors are strongly correlated and this makes the linear system sensitive to the fluctuations of the calibration samples. In our case, it means that the system is vulnerable to noise. Moreover, even though we have made efforts to control it, overfitting is always a potential problem unless the number of calibration samples is fairly large ($m > n$). To avoid these risks, it is prudent to reduce the system size from multi-thousand to several tens, and then apply linear regression on the reduced system. The methods we used for this purpose are described in the following sections.
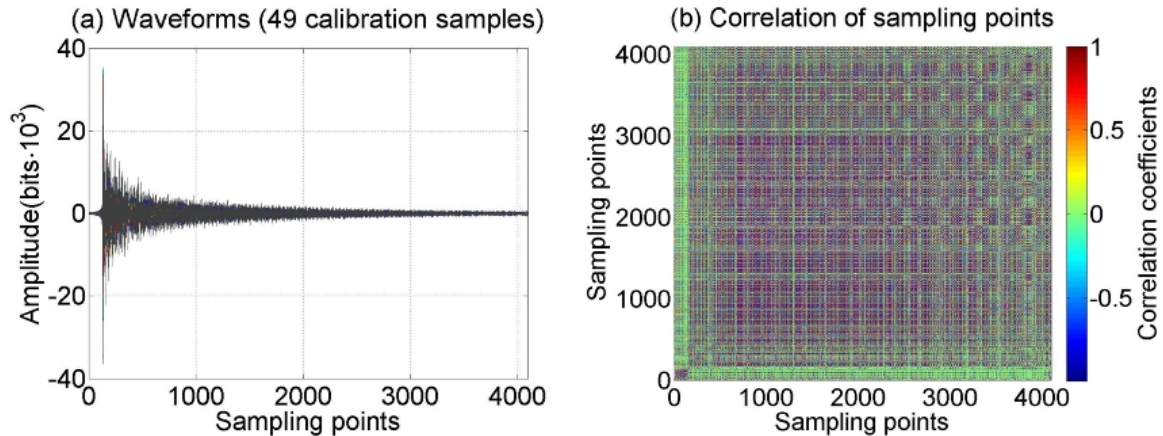
![EuCARD logo]

**HOM ELECTRONICS AND CODE TO
PROBE BEAM CENTRING
ON 3.9 GHZ CAVITIES**

Doc. Identifier:

EuCARD-D10 **5 1-report-FINAL-
RMJ**

Date: 17/07/2013

Fig. 47 (a) Waveforms of 49 calibration samples; (b) Correlation coefficients between each regressor of DLR.

5.1.3. Singular value decomposition

In order to reduce the dimension of the system, a method known as Singular Value Decomposition (SVD) is used to find a small number of prominent components from the waveform matrix A. In general, SVD looks for patterns of a matrix in terms of SVD modes without the knowledge of any physical parameters (like dipole mode frequency, quality factor, beam position, etc.). Those SVD modes are natural groupings of the signal matrix, which are not clearly visible or explicitly defined in the matrix itself.

Applying SVD, the matrix A is decomposed into the product of three matrices,

$$A = U \cdot S \cdot V^T \tag{17}$$

where V^T indicates the transpose of V. The columns of U and V are singular vectors of A, which form the bases of the decomposition. S is a diagonal matrix whose non-zero elements are known as singular values. Fig. 48(a) shows the singular value of each SVD mode decomposed from the calibration samples. It can be seen that the first few SVD modes have relatively large singular values, in other words, they are the dominant patterns of matrix A.
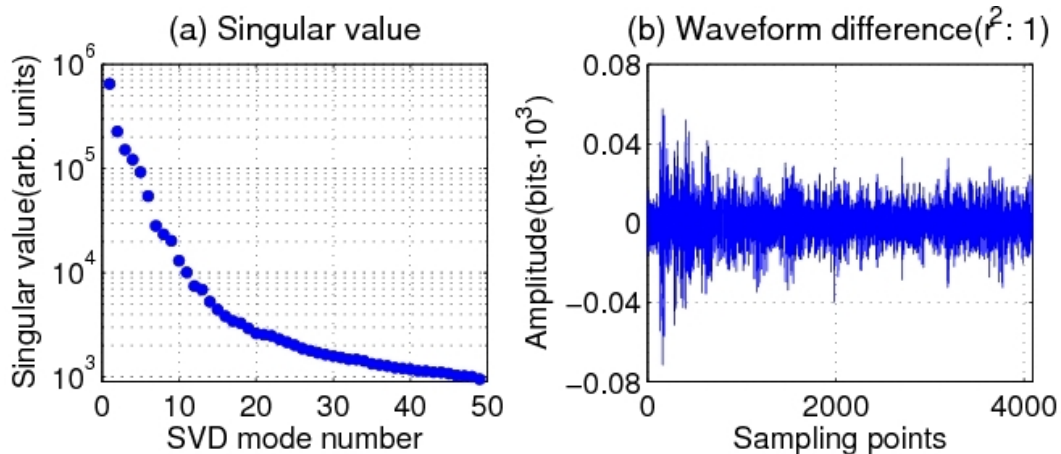

Fig. 48 (a) Singular value of each SVD mode; (b) Difference of the original and the reconstructed waveform using the first 26 SVD modes. Note the scale of the waveform amplitude when comparing with Fig. 42(a).

Each of the SVD modes can be used to produce a waveform matrix by

EuCARD

**HOM ELECTRONICS AND CODE TO
PROBE BEAM CENTRING
ON 3.9 GHZ CAVITIES**

Doc. Identifier:

EuCARD-D10 **5 1-report-FINAL-
RMJ**

Date: 17/07/2013

$$A_i = U_i \cdot S_{ii} \cdot V_i^T \tag{18}$$

where U_i is the ith column of U, and V_i^T is the ith row of V^T. S_{ii} denotes the ith diagonal element of S. A_i has the same size as the original waveform matrix A. Fig. 49 shows one waveform for each of the first nine A_i. The approximation A_{reco} can be calculated by simply summing over the related A_i's by

$$A_{reco} = \sum_{i=1}^{p} A_i \tag{19}$$

Fig. 48(b) shows the difference between the original waveform A and A_{reco} for $p = 26$. One can see that the waveform can be well represented by using only the first 26 SVD modes, which is also illustrated by $r^2 \approx 1$. The choice of p will be discussed later.
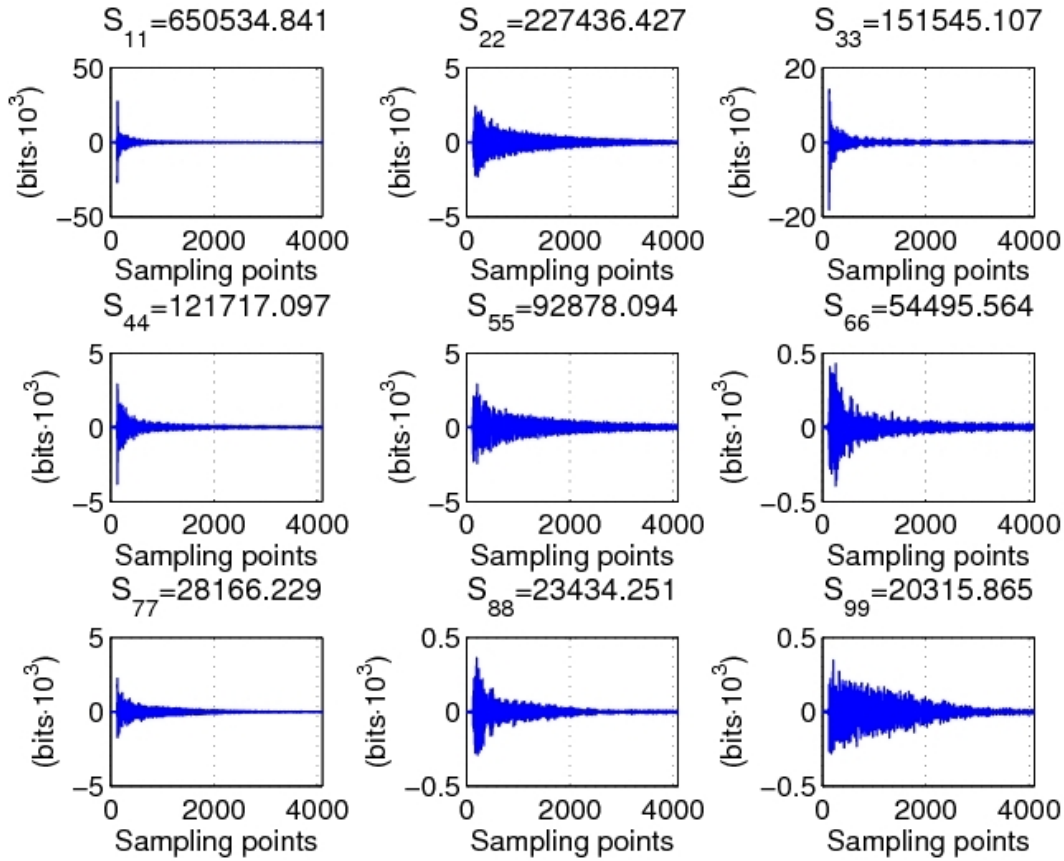

Fig. 49 Waveform reconstructed from each of the first nine SVD modes.

With the SVD base vectors from the decompositions of waveform matrix A, the amplitude of all SVD modes, $A_{svd, full}$, can be obtained for each beam position by

$$A_{svd,full} = A \cdot V = (A_1^{svd}, A_2^{svd}, \dots). \tag{20}$$

$A_i^{svd} \in R^{m \times 1}$ contains the mode amplitude for each beam position of the ith SVD mode. Fig. 50(a) shows the mode amplitude of the first 49 SVD modes with non-zero singular values obtained from the calibration samples. The correlation coefficient between each pair of SVD mode is also calculated using Eq. 16 by replacing a_i and a_j by A_i^{svd} and A_j^{svd} and it is shown

**HOM ELECTRONICS AND CODE TO
PROBE BEAM CENTRING
ON 3.9 GHZ CAVITIES**

Doc. Identifier:

EuCARD-D10 **5 1-report-FINAL-
RMJ**

Date: 17/07/2013

in Fig. 50(b). The first SVD mode has relatively strong correlations with several SVD modes. This is because the mean of the 49 calibration waveforms is not zero.
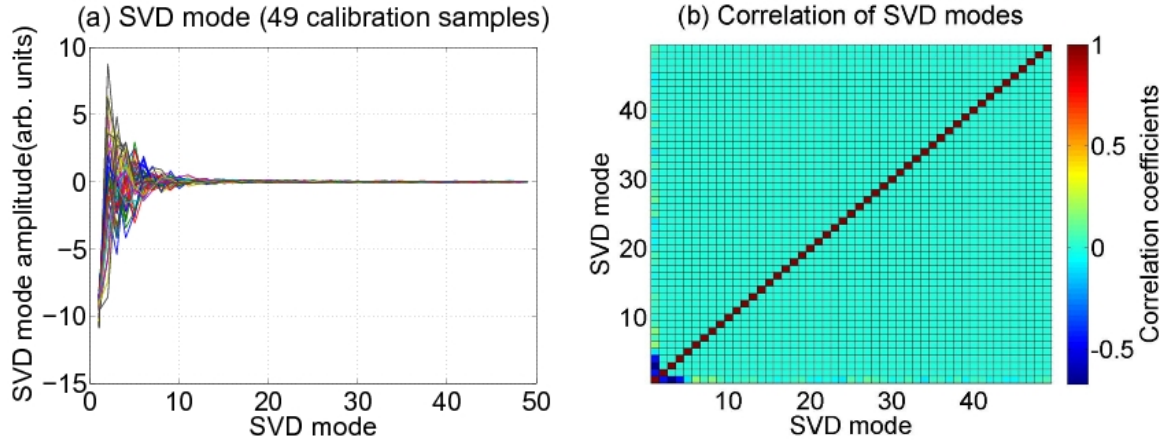

Fig. 50 SVD mode amplitudes and their correlations.

Along with a column of 1, $I \in R^{m \times 1}$, representing the intercept term, we use the first p ($p \leq m$) SVD modes to build the SVD mode amplitude matrix A_{svd}:

$$A_{svd} = (I, A_1^{svd}, A_2^{svd}, \ldots, A_p^{svd}). \tag{21}$$

The size of the matrix A_{svd} is significantly smaller (p+1 columns, representing p SVD modes and 1 intercept term) compared to the original waveform matrix A (4097 columns, representing 4096 sampling points and 1 intercept term). Replacing A by A_{svd} in the regression (Eq. 13), the linear system composed by A_{svd} and B is now over-determined, and has a best solution in a least square sense. The prediction for the validation samples has two steps: first, project A onto the base vectors obtained from calibration samples to get the amplitude of the SVD modes using Eq. 20; second, predict positions using the SVD amplitude matrix and the coefficient matrix M.

The contribution of combining the first p SVD modes to determine the transverse beam position x and y is measured by the RMS error as shown in Fig. 51. Zooming into the region where $12 \leq p \leq 32$, the E_{RMS} of x and y for validation samples are shown in Fig. 52. Using the first 26 SVD modes is seen to give an optimal performance for both x and y plane. This confirms, with Fig. 48, that the first few SVD modes contain the majority of the beam position information.
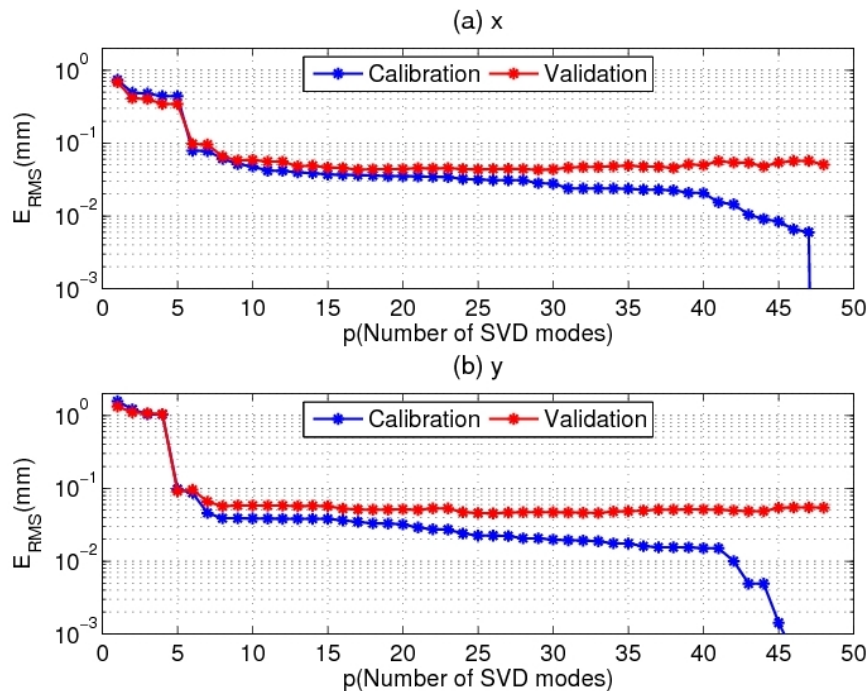
Fig. 51 Contribution of the first p SVD modes to determine the transverse beam position x and y measured by E_{RMS}.
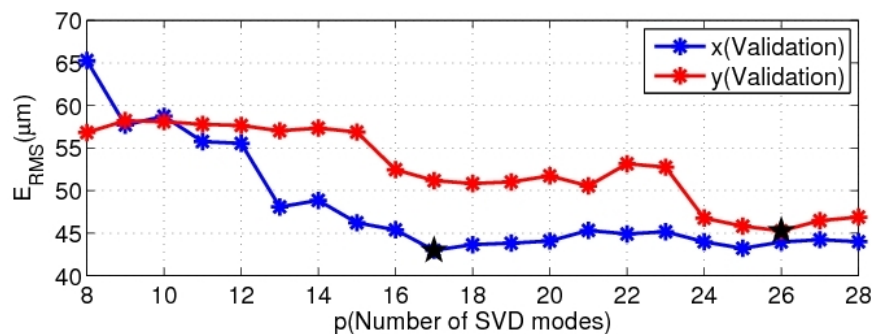
Fig. 52 Contribution of the first p SVD modes ($12 \leq p \leq 32$) to determine the transverse beam position x and y measured by E_{RMS}.

Fig. 53 shows the HOM response from calibration and validation samples by using the first 26 SVD modes to determine the transverse beam position *x* and *y*. The RMS errors remain small and comparable for calibration and validation samples as shown in Fig. 54. The RMS error is 44 µm for *x* and 45 µm for *y* when predicting positions from validation samples.

**HOM ELECTRONICS AND CODE TO
PROBE BEAM CENTRING
ON 3.9 GHZ CAVITIES**

Doc. Identifier:

EuCARD-D10 **5 1-report-FINAL-
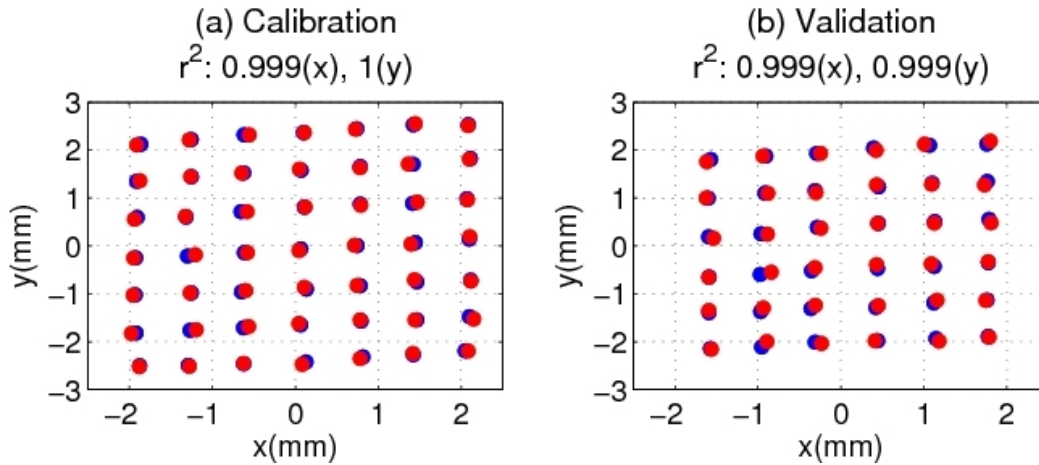RMJ**

Date: 17/07/2013

Fig. 53 Measurement (blue) and prediction (red) of the transverse beam position from calibration and validation samples. The method applied is SVD with the first 26 SVD modes.
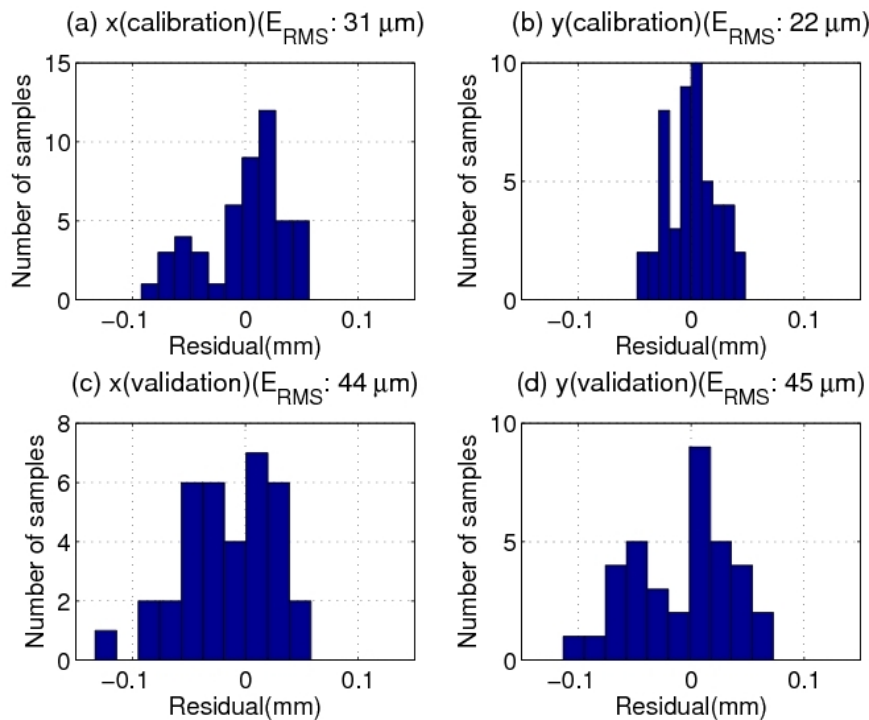
Fig. 54 Difference of measured and predicted transverse beam position from calibration and validation samples. The method applied is SVD with the first 26 SVD modes.

5.1.4. *k*-means clustering

An information redundancy is present in the linear system composed of A (Eq. 11) and B (Eq. 12), as the regressors a_i's from the waveform matrix A are highly correlated (Fig. 47). A technique named k-means clustering is used in order to group the data into a few cohesive clusters. Each a_i is considered as one point in the m-dimensional space, and the goal is to find k groups of points based on Euclidean distance. The cluster centroid μ_j is defined as the average value of a_i's

HOM ELECTRONICS AND CODE TO
PROBE BEAM CENTRING
ON 3.9 GHZ CAVITIES

Doc. Identifier:

EuCARD-D10 **5 1-report-FINAL-RMJ**

Date: 17/07/2013

$$\mu_j = \frac{1}{M} \sum_{i=j_1}^{j_M} a_i$$

(22)

where $(j_1, j_2, ..., j_M)$ are M indices of the m-dimensional points a_i's which belong to the j_{th} cluster whose centroid is μ_j. Fig. 55 shows 22 clusters in red partitioned from the calibration samples in blue for one beam position. The values of the corresponding 22 centroids are shown in Fig. 56(a) for all 49 beam positions. The correlation coefficients of these clusters can be calculated by replacing a_i with μ_j in Eq. 16 and are shown in Fig. 56(b). As expected, correlations can be observed among clusters.
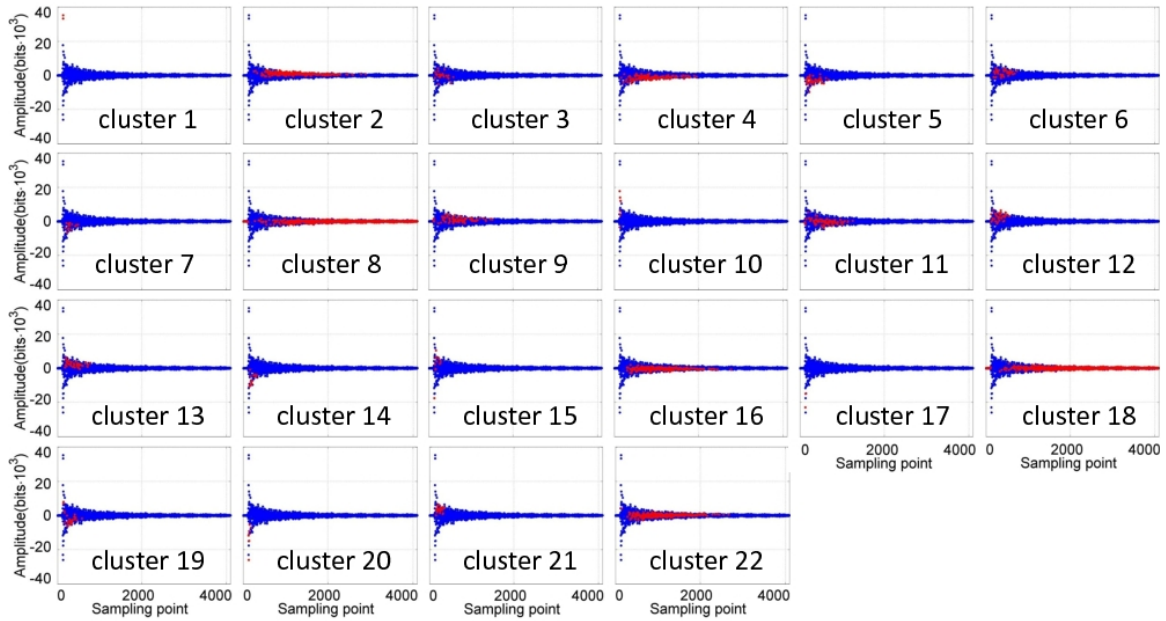

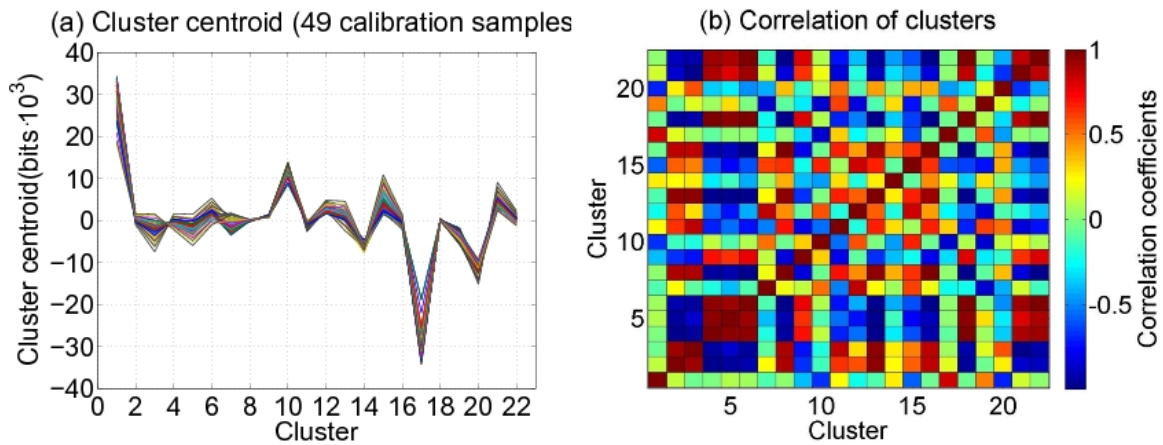*Fig. 55 22 clusters (red) partitioned from the calibration samples (blue) for one beam position.*

Fig. 56 Cluster centroids and their correlations.

The contribution of different number of clusters to determine the transverse beam position x and y is measured by the RMS error as shown in Fig. 57. Using 22 clusters is seen to give an optimal performance for both x and y.

**HOM ELECTRONICS AND CODE TO
PROBE BEAM CENTRING
ON 3.9 GHZ CAVITIES**

Doc. Identifier:

EuCARD-D10 **5 1-report-FINAL-
RMJ**

Date: 17/07/2013
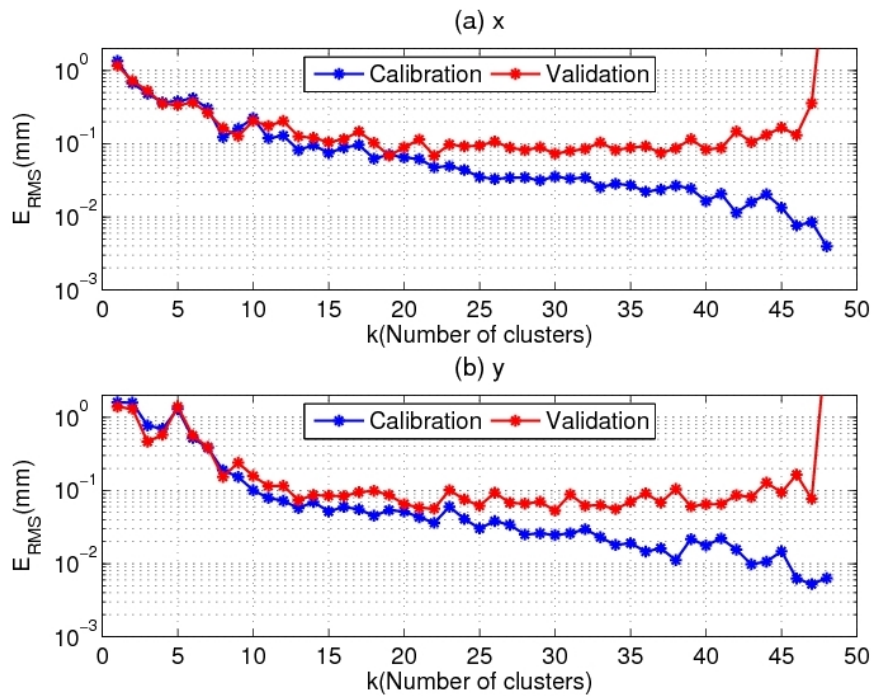
Fig. 57 Different number of clusters to determine the transverse beam position x and y measured by E_{RMS}.

Fig. 58 shows the HOM response from calibration and validation samples by using 22 clusters to determine the transverse beam position *x* and *y* respectively. The RMS errors remain small and comparable for calibration and validation samples as shown in Fig. 59. The RMS error is 68 μm for *x* and 56 μm for *y* when predicting positions from validation samples.

Fig. 58 Measurement (blue) and prediction (red) of the transverse beam position from calibration and validation samples. The method applied is k-means clustering with 22 clusters.

HOM ELECTRONICS AND CODE TO
PROBE BEAM CENTRING
ON 3.9 GHZ CAVITIES

Doc. Identifier:

EuCARD-D10 **5 1-report-FINAL-RMJ**

Date: 17/07/2013

Fig. 59 Difference of measured and predicted transverse beam position from calibration and validation samples. The method applied is k-means clustering with 22 clusters.

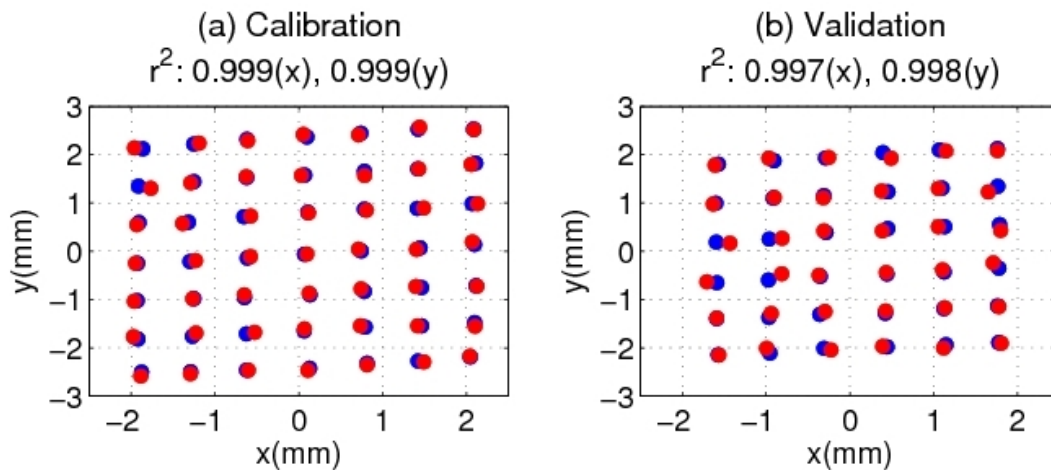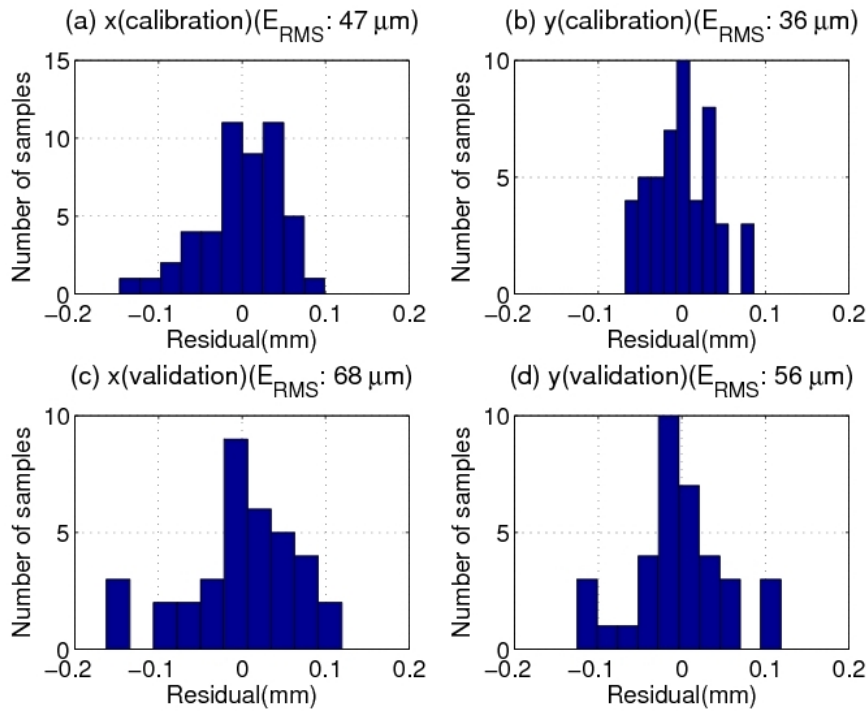## 5.2. PERFORMANCE EVALUATION

The performance of the three methods used to extract the beam position described in the previous section is evaluated in this section by two different techniques: the fixed sample split and cross-validation. A figure of merit, position resolution, is defined as the RMS error when predicting the validation samples (Eq. 15).

5.2.1. Fixed sample split

For the fixed sample split shown in Fig. 42(b), the position resolutions obtained from the three different methods are listed in Table 3 along with the calibration RMS errors. The RMS errors are comparable for DLR and SVD of both calibration and validation samples. Both methods suggest an approximately 50 μm position resolution. The *k*-means clustering suggests a worse resolution of 60 – 70 μm.

Table 3 Direct comparison of DLR, SVD and k-means clustering for the fixed sample split.

	Calibration		Validation	
	$E_{RMS}(x)$	$E_{RMS}(y)$	$E_{RMS}(x)$	$E_{RMS}(y)$
DLR	30 μm	25 μm	40 μm	50 μm
SVD	31 μm	22 μm	44 μm	45 μm
Clustering	47 μm	36 μm	68 μm	56 μm

EuCARD

**HOM ELECTRONICS AND CODE TO
PROBE BEAM CENTRING
ON 3.9 GHZ CAVITIES**

Doc. Identifier:

EuCARD-D10 **5 1-report-FINAL-
RMJ**

Date: 17/07/2013

5.2.2. Cross-validation

Until now, our analysis is based on a specific sample split (Fig. 42(b)). To remove the sample dependence, a technique named cross-validation is used. As our total sample size is quite small (85 samples), we use the technique called leave one-out cross-validation (LOOCV). For each sample split, LOOCV uses only one sample from the total samples as validation, and the remaining 84 samples are used for calibration. This is repeated 85 times such that each sample out of all the samples is used once for validation. The RMS error is then calculated on the residuals for the validation sample from all 85 different sample splits.
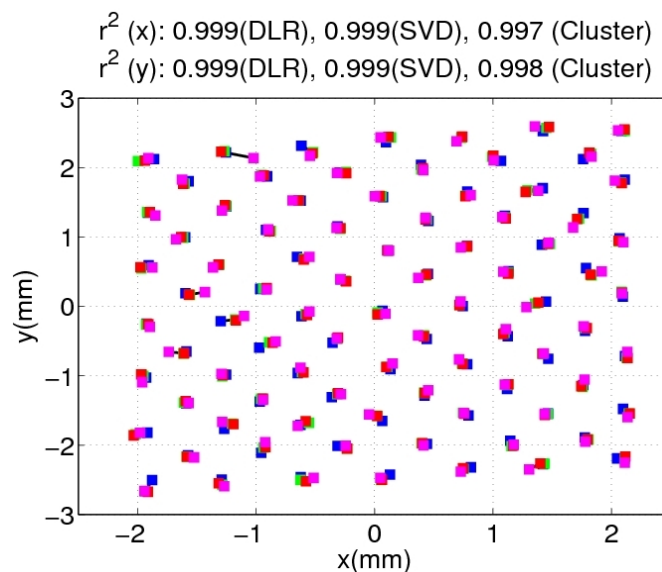

Fig. 60 Measurement (blue) and prediction of the transverse beam position from each of 85 validation samples using LOOCV. The DLR is in red. The SVD is in green with the first 26 SVD modes. The k-means clustering is in magenta with 22 clusters. Points connected with black lines belong to the same beam position.

Fig. 60 shows the measurement and the prediction of each sample when it is used for validation in that specific sample split. The methods applied are DLR (red), SVD (green) with the first 26 SVD modes, and k-means clustering (magenta) with 22 clusters. Fig. 61 shows the corresponding residuals for these three methods. The sample-independent RMS errors are listed in Table 4. Since the calibration samples for each of the 85 sample splits are similar, the RMS error for the validation sample from all 85 sample splits is a good estimation of the position resolution. The results are similar to the fixed sample split case shown in Table 2. Although the results are comparable for all three methods, SVD and *k*-means clustering are far more efficient than DLR in computing calibration coefficients, since the number of unknown variables is much smaller, as shown in Table 4. However, once the calibration matrix *M* is obtained, the time required for position prediction is generally equally fast.
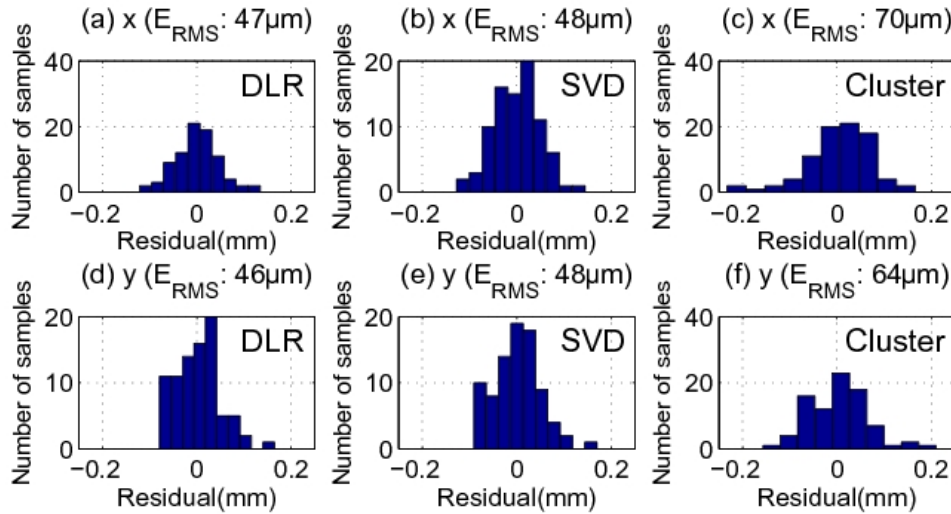
Fig. 61 Difference of measured and predicted transverse beam position from each of 85 validation samples using LOOCV.

Table 4 Direct comparison of DLR, SVD and k-means clustering using cross-validation.

	$E_{RMS}(x)$	$E_{RMS}(y)$	Number of unknowns
DLR	$47\ \mu m$	$47\ \mu m$	4097
SVD	$51\ \mu m$	$48\ \mu m$	27
Clustering	$70\ \mu m$	$64\ \mu m$	23

5.3. SUMMARY OF STATISTICAL METHODS

We have studied various methods to extract the transverse beam position from the HOMs excited by an electron beam in a third harmonic superconducting cavity. A linear system has been composed from HOM waveforms in the fifth dipole band with frequencies in the range 9040 – 9078 MHz and measured beam positions. DLR on the entire waveforms suggests a position resolution of 40 μm for x and 50 μm for y. Due to the large number of sampling points occurred from the waveforms, the system has a considerable number of unknown variables to be determined. This leads to a long computation time in the calibration phase. Therefore, two methods are used to reduce the dimension of the system effectively: SVD and k-means clustering. SVD gives a comparable position resolution to DLR of 44 μm for x and 45 μm for y, while k-means clustering provides a reasonable resolution of 68 μm for x and 56 μm for y. In order to eliminate the sample dependence, a cross-validation technique has been applied with these three methods. The RMS prediction error of approximately 50 μm can be achieved by both DLR and SVD, while a 30% - 40% worse precision is suggested by the k-means clustering.

In this study, SVD is seen to be an effective and computation efficient method to reduce the system dimension while preserving good position resolutions in both x and y. Therefore it has been decided to implement SVD into the final HOM electronics for beam position diagnostics in third harmonic cavities for FLASH and the European XFEL.

Doc. Identifier:

EuCARD-D10 5 1-report-FINAL-RMJ

Date: 17/07/2013

**HOM ELECTRONICS AND CODE TO
PROBE BEAM CENTRING
ON 3.9 GHZ CAVITIES**

6. CONCLUSION AND FUTURE WORK

We report the design of a higher order mode beam position monitor (HOMBPM) using dipole modes in third harmonic 3.9 GHz accelerating cavities. HOMBPM has the capability of measuring beam positions inside the accelerating module without additional vacuum components. Conventional BPMs fall short of providing this information directly. The amplitude of the dipole mode has a linear dependence on the transverse position of the excitation bunch. This enables the diagnostics by measuring these dipole modes extracted from HOM couplers.

Although the principle of beam diagnostics with HOM has been proved in the TESLA 1.3 GHz cavity at FLASH, the realization of a HOMBPM in 3.9 GHz cavities is considerably more challenging due to the complexity present in the HOM spectrum. The first obstacle is to find suitable dipole modes. The ideal candidate is the mode which has strong coupling to the beam (large R/Q value), since it can deliver higher position resolution. In 3.9 GHz cavities, the first two dipole bands contain modes with large R/Q's. However, these modes are not confined inside each cavity but propagating through the entire four-cavity module. HOMBPM using these multi-cavity modes can only deliver the beam position in a four-cavity module sense. The second obstacle is that modal frequencies are unpredictable. This inevitably adds complexities to the electronics design for each HOM coupler. Some modes in the fifth dipole band are found to be trapped inside each cavity and could be used for local position diagnostics. The third obstacle is that these modes are located in an upper frequency range (~9 GHz) and have only weak coupling to the beam (small R/Q). The former will require careful electronics design and the latter will impact the position resolution of the HOMBPM.

In order to overcome or mitigate these obstacles, extensive studies have been conducted prior to building the HOMBPM electronics. These are eigenmode simulations, measurements of the scattering parameter S_{21}, beam-based HOM spectra measurements and the study of dipole dependence on the beam offset with a spectrum analyzer. Three modal options promising for beam diagnostics have been narrowed down: localized dipole beam-pipe modes at approximately 4 GHz, coupled cavities modes in the first two dipole bands in the range of 4.5 - 5.5 GHz and trapped cavity modes in the fifth dipole band at approximately 9 GHz. In order to evaluate the position resolution using these options, a test electronics consisting of a downmixer and digitizer was designed and built by Fermilab. Various frequency bands of these three options have been studied with the test electronics. In the end, two types of HOMBPM appear to be feasible. The first type is based on a four-cavity module using coupled cavity modes with large R/Q's in the first two dipole bands. Since the 3.9 GHz four-cavity string is not significantly longer than one TESLA 1.3 GHz cavity (approximately 1.3 times), the beam position determined in a module sense is still useful. In addition, coupled strongly to the beam, these modes are essential for beam alignment to minimize HOM power. The second type is based on each cavity using localized cavity modes in the fifth dipole band. Moreover, we utilize the signal of a complete band of frequencies rather than a specific dipole mode as used in HOMBPM system for TELSA 1.3 GHz cavities. This has been proved to be able to not only improve the resolution previously limited by modes with small R/Q's, but also accommodate the individual modal frequencies among couplers.

Various data analysis methods have been applied to effectively correlate HOMs to the beam offset. A Direct Linear Regression (DLR) on the HOM signals is able to predict beam positions accurately but fell short of computation efficiency due to a considerable number of sampling points of the HOM signals. Thus two statistical methods have been applied and successfully reduced the dimension of the HOM signal without losing the concealed beam position information: Singular Value Decomposition (SVD) and *k*-means Clustering. Then both accurate position predictions and computation efficiencies have been achieved along with a noise reduction as a by-product.

For the case of only one bunch in the train, our present experiments with the test electronics suggest a resolution of 50 μm accuracy in predicting local beam position in the cavity and a global resolution of 20 μm over the complete module. For multi-bunch operation, a non-degenerate resolution can be achieved when diagnosing the first bunch in the train by using a proper time window on the HOM signals. Due to an overlap of HOM signals with the following bunches, degeneration of position resolution can be foreseen for the trailing bunches in the train.

There are three highlights present in this work. This is the first time that dependencies of HOMs on beam offset have been observed in third harmonic 3.9 GHz cavities. A new analysis method named *k*-means Clustering has been successfully implemented in the HOM-based beam diagnostics for the first time. This is also the first time that three data analysis techniques (DLR, SVD and *k*-means Clustering) have been compared directly in terms of performance and model complexity in the study of beam diagnostics with HOMs.

Future Studies on HOMBPM

Based on the extensive evaluations of various frequency bands using the test electronics, a set of dedicated electronics is being built using modes in the second dipole band and the fifth dipole band, in order to facilitate beam position measurements over the whole third harmonic module with high resolution, and localized within individual 3.9 GHz cavities with reasonable resolution. The centre frequency has been chosen to be 5440 MHz for the coupled modes and 9060 MHz for the trapped cavity modes both with 20 MHz bandwidth. For FLASH, we will equip two HOM couplers for the 5440 MHz and six couplers for the 9060 MHz except the first and the last HOM couplers in the module. We plan to evaluate the HOMBPM system and integrated into FLASH control system in 2013.

As observed in the previous TESLA 1.3 GHz cavity case, the calibration of the HOMBPM was only stable for 1 – 2 days. This issue need to be understood and is planned to be studied for both 1.3 GHz and 3.9 GHz HOMBPM system. This is essential for a stable operation of an online beam diagnostics instrument. Based on the results obtained so far, it has been planned to build similar HOMBPM system for the European XFEL third harmonic module consisting of eight 3.9 GHz cavities.

**HOM ELECTRONICS AND CODE TO
PROBE BEAM CENTRING
ON 3.9 GHZ CAVITIES**

Doc. Identifier:
EuCARD-D10 **5 1-report-FINAL-
RMJ**

Date: 17/07/2013

ANNEX: GLOSSARY

Acronym	Definition
HOM	Higher Order Mode
HOMBPM	HOM-based beam position monitor
R/Q	Coupling factor between beam and HOMs
SVD	Singular Value Decomposition
ACC39	Accelerating module in FLASH linac, containing 3.9 GHz cavities

http://cern.ch/EuCARD/about/glossary/